Effect of strain path change during cold rolling on the evolution of deformation and recrystallization textures of high purity Nickel

Mohit Joshi

A Dissertation Submitted to
Indian Institute of Technology Hyderabad
In Partial Fulfilment of the Requirements for
The Degree of Master of Technology

भारतीय प्रौद्योगिकी संस्थान हैदराबाद
Indian Institute of Technology Hyderabad

Department of Material Science and Engineering

July, 2012

Declaration

I declare that this written submission represents my ideas in my own words, and where others' ideas or words have been included, I have adequately cited and referenced the original sources. I also declare that I have adhered to all principles of academic honesty and integrity and have not misrepresented or fabricated or falsified any idea/data/fact/source in my submission. I understand that any violation of the above will be a cause for disciplinary action by the Institute and can also evoke penal action from the sources that have thus not been properly cited, or from whom proper permission has not been taken when needed.
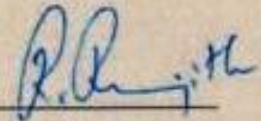
_____

(Signature)

Mohit Joshi
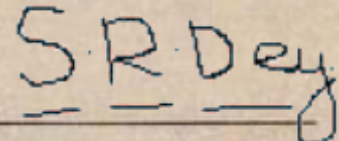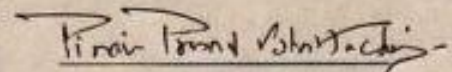MS10M04

Approval Sheet

This thesis entitled **Effect of strain path change during cold rolling on the evolution of deformation and recrystallization textures of high purity Nickel** by **Mohit Joshi** is approved for the degree of Master of Technology from IIT Hyderabad.

Dr. R. Ranjith
(Department of Materials Science and Engineering)
Examiner

Dr. S. R. Dey
(Department of Materials Science and Engineering)
Examiner

Dr. P. P. Bhattacharjee
(Department of Materials Science and Engineering)
Adviser

Dr. Raja Banerjee
(Department of Mechanical Engineering)
Chairman

Acknowledgements

Working the M Tech thesis has been a real learning experience for me. This dissertation has been one of the significant academic achievements for me. It is a pleasure to thank many people for making my M Tech a memorable experience.

I am deeply grateful to my thesis guide **Dr. Pinaki Prasad Bhattacharjee**, H.O.D, Department of Material Science& Engineering, for providing excellent guidance, consistent encouragement, inspiration and motivation to stay focused throughout the research work. Without his invaluable guidance, this work would never have been a successful one. I also want to thank **Professor U.B Desai**, Director, IIT Hyderabad for kindly allowing me to perform experimental work in IIT Bombay.

I would like to thanks **Professor N. Tsuji**, Kyoto University, Japan for his kind permission to carry out the rolling of the specimens and **Professor I. Samajdar**, IIT Bombay, India, for allowing me to perform characterization of the deformed materials.

I want to thank Ph. D scholars **Mr. J. R. Gatti** and **Mr. M. Z. Ahmed** for their co-operation in my experimental work.

I would like to thank Faculty member, Research scholars and M Tech colleague of Department of Material Science& Engineering for their help and support.

I am also thankful to all my friends at IIT Hyderabad for providing a stimulating and fun environment and making my stay in the institute campus a pleasure.

Lastly, and most importantly, I want to thank my parents, **Smt. Durga Joshi** and **Sh. R. C. Joshi** for their blessings, love and support.

Dedicated to

My Parents

Abstract

The effect of strain path change during cold rolling and subsequent annealing on the evolution of microstructure, texture and hardness properties of high purity nickel (~99.7%, average size ~ 36 μm) has been studied in the present work. Strain path change is achieved by employing two different rolling routes, namely, straight cold rolling (SCR) and cross cold rolling (CCR) in the present investigation. The rolling direction is kept constant throughout the deformation process in SCR route but during CCR processing the rolling direction (RD) and the transverse direction (TD) are mutually interchanged in every consecutive pass by rotating the sample around the normal direction (ND). Nickel sheets were deformed up to 90% reduction in thickness using the above two processing routes.

SCR processing route results in a lamellar microstructure and pure metal or copper type deformation texture characterized by the strong presence of S ({123}<634>), Cu ({112}<111>) and B_s ({110}<112>) orientations. The CCR processed microstructure, in contrast, is characterized by the presence of microstructural inhomogeneities, such as, intersecting shear band and localized intensely sheared regions. The texture of CCR processed material is characterized by strong presence of the Bs and BsND components, such as ($\{011\} < 21\ \overline{13}\ 13 >$) and ($\{011\} < 1\overline{1}1 >$).

The CCR processed material was recrystallized at different temperatures ranging between 400° to 800°C. Up on annealing at 400°C, ND||[111] fiber could be observed in the microtexture which originated from the twinning of the recrystallized TD-rotated cube ($\{027\}<0\overline{7}2>$) grains. The fiber was weakened after annealing at 800°C due to the decreased propensity for twin formation and the microtexture was found to be weak and diffuse. EBSD investigation on early recrystallization stages indicates absence of preferential nucleation of near cube grains. Instead, presence of TD-rotated cube grains and their twins in agreement with a weak cube texture formation in annealed CCR processed nickel.

The development of recrystallization texture in the CCR processed materials was found to be in stark contrast to the recrystallization texture of SCR processed materials where strong cube texture could be observed and also reported almost universally. The internal structure and local misorientation environment of cube regions in CCR processed nickel appear to be important factors but should be investigated further in the future works.

Nomenclature

SCR- Straight Cold Rolling

CCR- Cross Cold Rolling

GO map- Grain Orientation map

GB map- Grain Boundary map

ODF- Orientation Distribution Function

PF- Pole Figure

FCC- Face Centered Cubic

RD- Rolling Direction

TD- Transverse Direction

ND- Normal Direction

HAGB- High Angle Grain Boundary

LAGB- Low Angle Grain Boundary

EBSD- Electron Back Scattered Diffraction

VH- Vickers Hardness

θ_{mis}- Misorientation of Grain boundaries

C- Cube orientation {001} <100>

C^T- Twinned cube orientation {221} <1$\bar{2}$2>

C_{TD}- TD –rotated cube orientation {027} <0$\bar{7}$2>

C_{TD}^T- Twinned TD –rotated cube orientation {445} <13$\bar{2}\bar{3}$8>

C_{RD}- RD –rotated cube orientation {011} <100>

C_{RD}^T- Twinned RD –rotated cube orientation {185} <21$\bar{2}$>

Cu- Copper orientation {121} <1$\bar{1}$1>

S- S orientation {123} <634>

B_s- Brass orientation {011} <2$\bar{1}$1>

B_s^{ND}- ND rotated Brass orientation {011} <1$\bar{1}$1>

G- Goss orientation {013} <100>

G^{ND}- ND rotated Goss orientation {101} <$\bar{1}$01>

T- Taylor orientation {113} <$\bar{3}\bar{3}$2>

Contents

Chapter 1

Introduction

1.1   Overview

Deformation processing of materials is usually accompanied by the development of characteristic microstructures and crystallographic textures which in turn influences the development of recrystallization texture during subsequent annealing. It is well known that deformation behaviour of materials is a function of processing parameters such as temperature, strain and strain rate but one of the important factor which also effects material behaviour and property but much lesser studied is how the deformation or strain is achieved i.e. the effect of *strain path*. For metals and alloys the strain path influences the development of microstructure and texture [1] which ultimately controls the properties of materials.

In case of rolling the effect of strain path change can be studied easily by changing the rolling and transverse direction (RD and TD, respectively) as shown in Fig. 1.1. Generally, strain path change in rolling is executed by employing two different types of rolling routes named as straight cold rolling (SCR) and cross cold rolling (CCR). In straight cold rolling the rolling direction (RD) is constant whereas in cross cold rolling sample is rotated by 90° around normal direction (ND) so that the transverse direction (TD) of previous rolling pass will become rolling direction of current rolling pass.
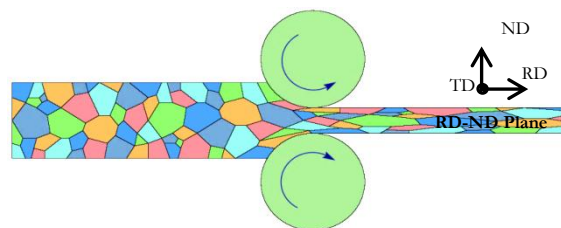
(a)
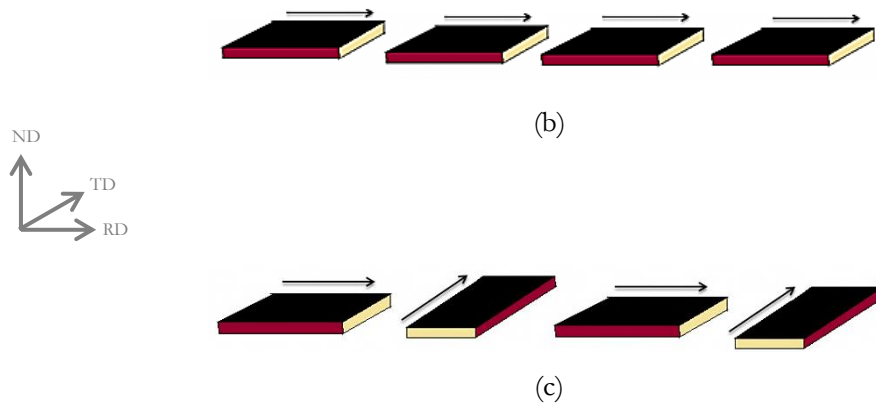
Figure 1.1: (a) Rolling process with reference directions as RD- Rolling Direction, ND-Normal Direction and TD-Transverse Direction [26] (b) Straight cold rolling (SCR) (c) Cross cold rolling (CCR). Black arrow represents the relative orientation of rolling direction of first pass.

1.2 Objective and Scope

The present work aims to investigate the effect of change in strain path on the development of microstructure and texture during heavy cold rolling and annealing of Nickel (99.7% purity) with relatively smaller starting grain size of 36 μm. For this purpose two different rolling routes, namely, SCR and CCR would be investigated followed by detailed characterization at different length scales using X-ray and electron back scatter diffraction techniques (XRD and EBSD, respectively). Finally, the results obtained are also proposed to be compared with coarse grain sized starting material (average grain size 800μm which has been undertaken in a parallel study) to clarify the effect of starting grain size.

Chapter 2

Literature Review

Considerable amount of work has been carried out on microstructural and textural evolution of face centered cubic (FCC) materials during rolling [2-6]. The common observation of rolling microstructure in FCC materials is the development of lamella structure with increasing strain and presence of deformation bands at higher strains. The rolling texture in FCC materials is usually characterized by the two incomplete fiber textures, α-fiber which extends from Goss orientation ({110} <001>) to brass orientation ({110} <112>) and β-fiber which extends from copper orientation (Cu component; {112} <111>) to brass orientation through S-orientation ({123} <634>) [4] as shown in Fig. 2.1. In FCC materials of high to medium stacking fault energy (SFE) (e.g. Al, Ni , Cu) the deformation texture is pure metal type texture characterized by the presence of Cu, S and Brass components whereas in low SFE materials deformation texture mainly composed of brass texture.

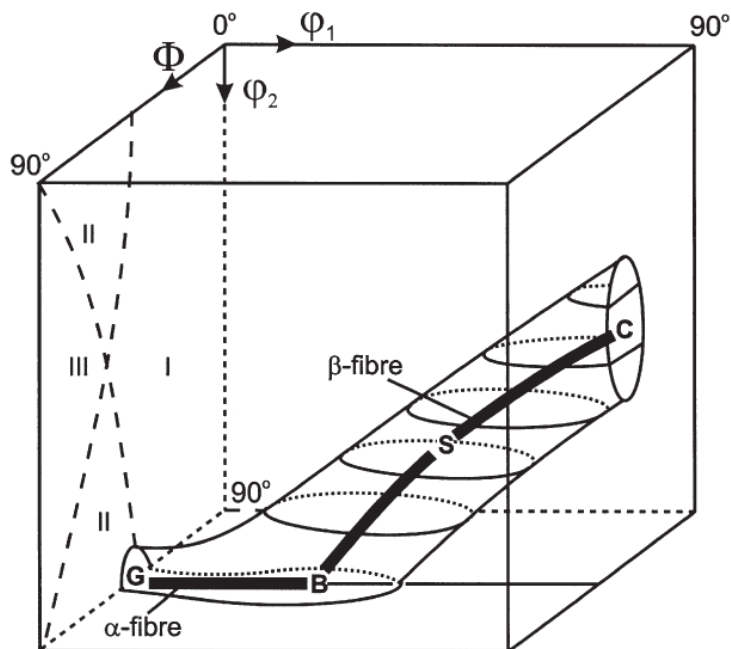Figure 2.1: Rolling texture in FCC Material showing β-fibre extends from Cu to Brass orientation through S orientation and α-fibre extends from Goss to Brass orientation in first subspace $(0 \leq \varphi_1 \leq 90°, 0 \leq \Phi \leq 90°, 0 \leq \varphi_2 \leq 90°)$ of three dimensional Euler space [4].

The deformation texture and microstructure in FCC materials will depend on stable orientations and dislocation substructures generated during deformation process [2, 6]. Usually with increase in strain the dislocation substructure size (like dislocation cells) reduces and texture becomes stronger. The evolution of deformation microstructure and texture depends on processing parameters including strain path, it is also found for rolling texture that it is very sensitive to strain path change [7]. In straight cold rolling the rolling texture becomes stronger with increasing strain whereas in cross cold rolling the substructures are rotated by 90^0 which make stable orientations and substructure of previous pass unstable along new rolling direction and weakens the previous pass texture. Limited studies available indicate that CCR processed microstructure and texture differ considerably from those of SCR. Fig. 2.2 shows the (111) pole figure of SCR and CCR processed nickel and copper which clearly shows the characteristics differences in the textures developed in the two different processing routes. It has been generally observed that brass and rotated brass components develop in CCR processed copper and nickel [7, 10] but need to be clarified in detail.
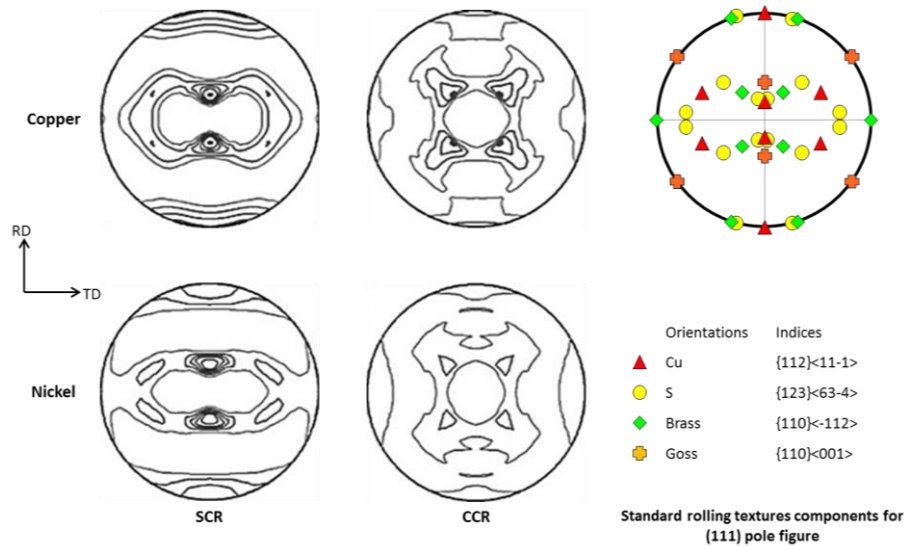
Figure 2.2: (111) pole figure of SCR and CCR processed samples with standard rolling texture components [7]

The difference in the deformation texture and microstructure due to CCR processing strongly affects the formation of recrystallization texture which has been studied in Aluminium alloys and other systems [8-10]. In medium to high stacking fault energy fcc materials a strong cube texture formation is observed following heavy cold deformation by SCR route and suitable annealing treatments which has been well documented in literature [11-18]. However, the usually strong cube recrystallization texture in aluminium alloys is suppressed by CCR [19] and it has been exploited to control the deep drawing properties of aluminium alloys. Similarly, the

12

usually strong recrystallization cube texture in copper is replaced by a single component {5 1 9} $< \bar{4} \ 11 \ 1>$ [20]. It is thus quite expected that CCR processing would also strongly affect the formation of recrystallization texture in nickel but yet to be clarified. The above unresolved issues essentially constitute the focus of the present work.

Chapter 3

Experimental Methods

3.1 Preparation of Starting Materials

In this research work high purity Nickel (99.7%) was selected for investigation. The starting material was prepared by deforming an as cast Ni slab of dimension ~ 160 mm ^{L} X 60 mm ^{W} X 10 mm ^{T} upto 50% reduction in thickness by multi pass cold rolling followed by annealing at 600^0C in a salt bath furnace for 1 hr. The process of preparing the starting materials is shown in the flow diagram in Fig. 3.1.
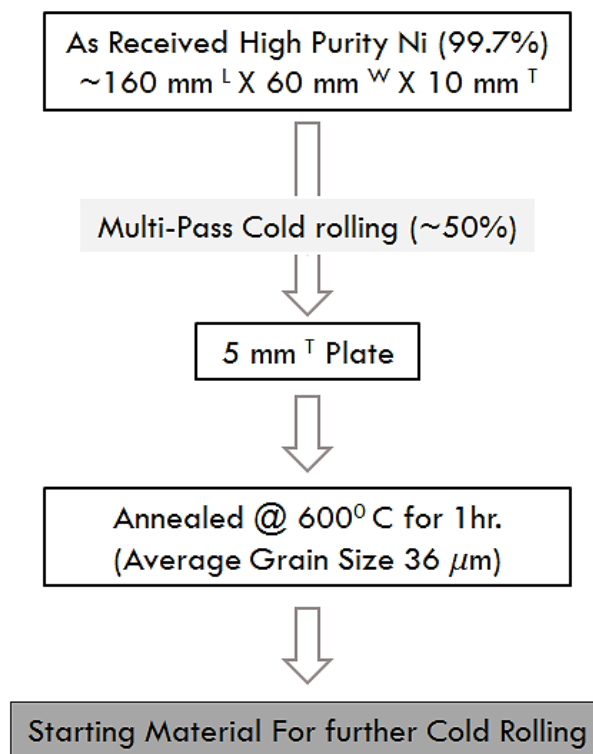
Figure 3.1: Process chart of starting material preparation from as received Nickel slab

3.2 Processing

3.2.1 Deformation Processing

To achieve different strain path, two different rolling routes namely straight cold rolling (SCR) and cross cold rolling (CCR) are employed to the starting material Nickel. In SCR the rolling direction was same in each pass whereas in CCR the rolling direction was rotated by 90^0 after every pass as shown in Fig 3.2. In both rolling routes nickel samples were deformed up to 90% reduction at room temperature in thickness using a laboratory scale rolling mill with well lubricated roll at room temperature.
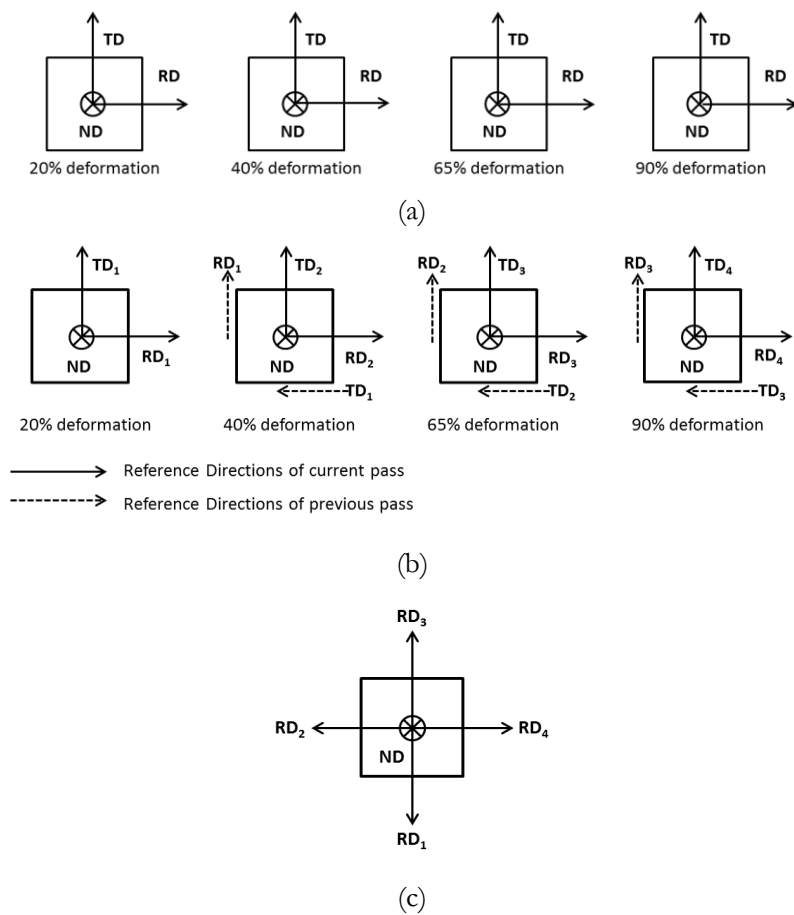
Figure 3.2: (a) Shows straight cold rolling (SCR), in which rolling direction (RD) remain same after every rolling pass, (b) shows cross cold rolling (CCR), in which rolling direction (RD) rotated by 90^0 anticlockwise around normal direction (ND) after every rolling pass and (c) shows relative orientations of rolling directions for each rolling pass in CCR.

3.2.2 Annealing

In order to clarify the effect of strain path change on the evolution of recrystallization microstructure and texture formation, small pieces of 90% deformed materials of each deformation routes were subjected to isochronal annealing treatment for one hour at 400°, 600° and 800°C using a salt bath furnace. The samples were immediately quenched in cold water following the recrystallization treatments.

3.3   Characterization

3.3.1 Sample preparation

The rolled samples were first cut in to small pieces using precision cutters Secotom-15 (Struers, Denmark) and Minitom, (Struers, Denmark). After the cutting operation, these samples were mechanically polished in three stages. In the first stage samples were sequentially polished using emery papers starting with coarse grit size (500) down to fine grit size (1200). In the second stage, these samples were polished by using 3μm (DiaDuo™, Struers, Denmark) diamond solution in a manual polishing machine Labpol -5 (Struers, Denmark) followed by polishing using 1μm colloidal silica in an automatic polishing machine Tegramin-25 (Struers, Denmark). Only 90% deformed samples were considered for bulk texture measurement by X-ray diffraction. The samples for XRD measurements were given a light surface etching on the rolling plane which was the plane of measurement following the mechanical polishing. For microstructural and textural characterization by electron back scatter diffraction (EBSD) the mechanically polished samples were further electropolished using a mixture of 90% methanol and 10% Perchloric acid as electrolyte. All polishing operations were carried out from the TD normal or RD-ND plane of rolled samples which was the plane under observation. For hardness measurements the specimen were mounted on a hot mounting press CitoPress -10 (Struers, Denmark) before the series of polishing operations described above. The hardness samples were mounted using a thermosetting resin (MultiFast™, Struers, Denmark) such that the RD-ND planed in exposed out from the mounted specimen as shown in Fig. 3.3.1.

Figure 3.3.1: The mounted specimen with RD-ND plane at top for hardness test, Mounted specimens: SCR 20%, SCR 40%, SCR 65%, and SCR 90% (from left to right).

3.3.2 Microstructural and Textural Characterization

The analysis of bulk texture is done by X-ray diffraction technique on a PANalytical MRD system using a Cu-Kα radiation (1.54 Å). For microtexture and macrotexture analysis the sample symmetry was assumed to be orthotropic since the imposed strain per rolling pass was relatively large (ε≥0.15).

The deformed samples were subjected to microstructural and microtexture characterization by electron backscatter diffraction (EBSD). The EBSD measurements were carried out in FEG SEM (FEI, Quanta, 3D FEG). The EBSD scan data acquired from RD-ND plane of rolled samples was analyzed by TSL-OIM™ software. A flow diagram summarizing the complete experimental work is shown in Fig. 3.3.2.
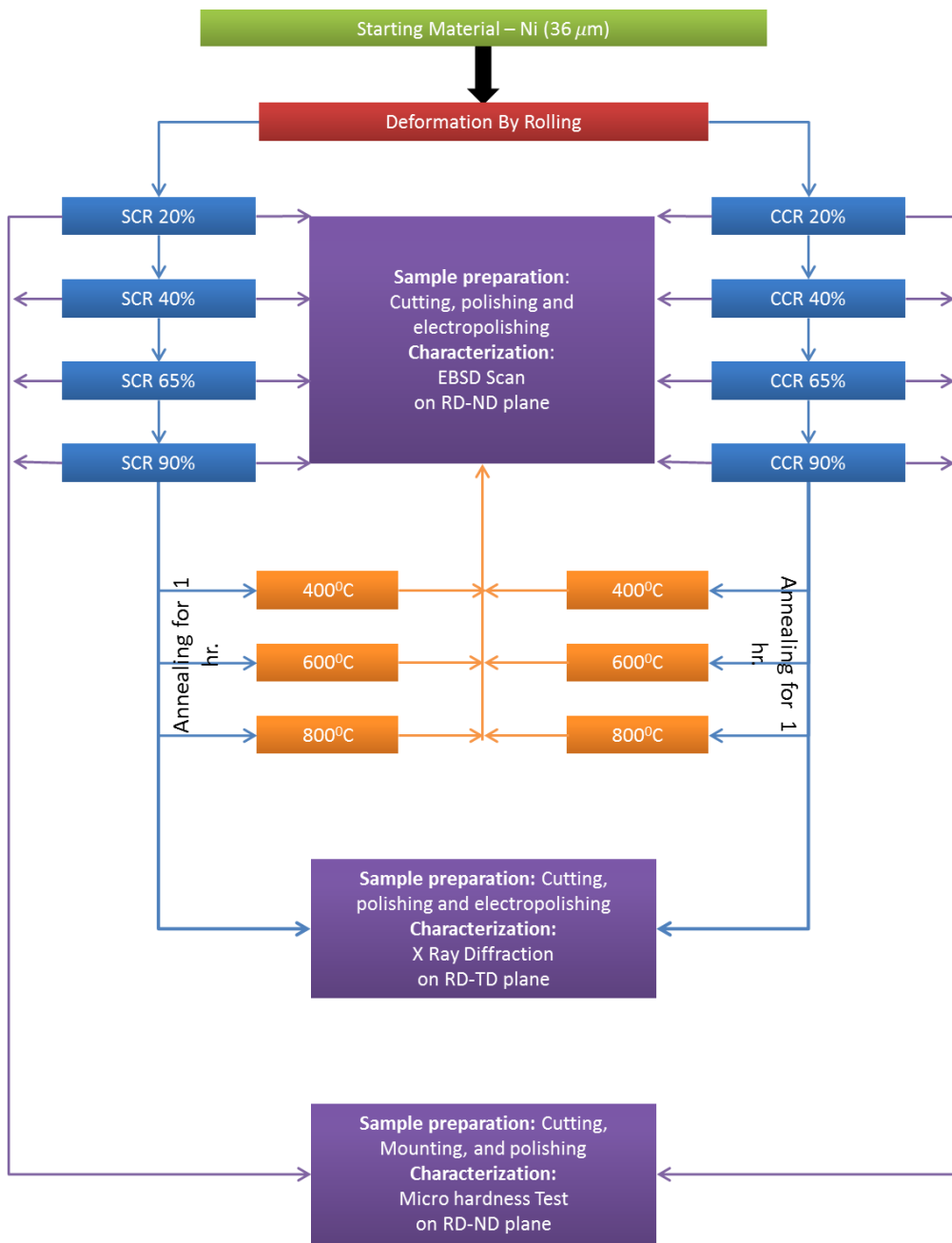
Figure 3.3.2 : Process chart of complete experimental work

The flowchart contains the following elements:

- Starting Material – Ni (36 μm)
- Deformation By Rolling

Left branch (SCR):
- SCR 20%
- SCR 40%
- SCR 65%
- SCR 90%

Right branch (CCR):
- CCR 20%
- CCR 40%
- CCR 65%
- CCR 90%

Sample preparation: Cutting, polishing and electropolishing
Characterization: EBSD Scan on RD-ND plane

Annealing for 1 hr. (left) — 400^{0}C, 600^{0}C, 800^{0}C
Annealing for 1 hr (right) — 400^{0}C, 600^{0}C, 800^{0}C

Sample preparation: Cutting, polishing and electropolishing
Characterization: X Ray Diffraction on RD-TD plane

Sample preparation: Cutting, Mounting, and polishing
Characterization: Micro hardness Test on RD-ND plane

3.3.3 Hardness Test

Microhardness test was carried out on the RD-ND plane of the deformed samples to characterize and compare their hardness properties. The hardness test was done using a load of 500 g and dwell time of 10 sec. per indentation. Five indentations were taken per sample with a gap of 250 µm and the average hardness value was determined. These tests were carried out on microhardness testing equipment, DuraScan (EMCOTEST™, Austria). A microindentation image of rolled sample is shown in Fig 3.3.3.
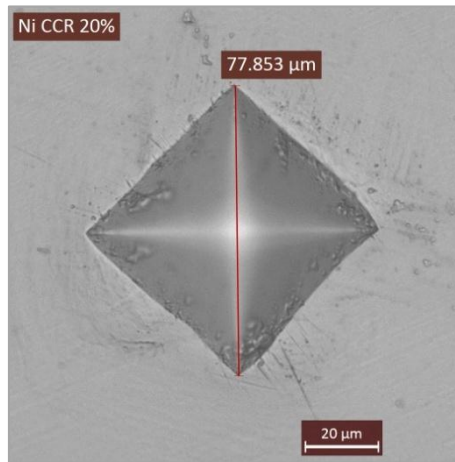
(a)
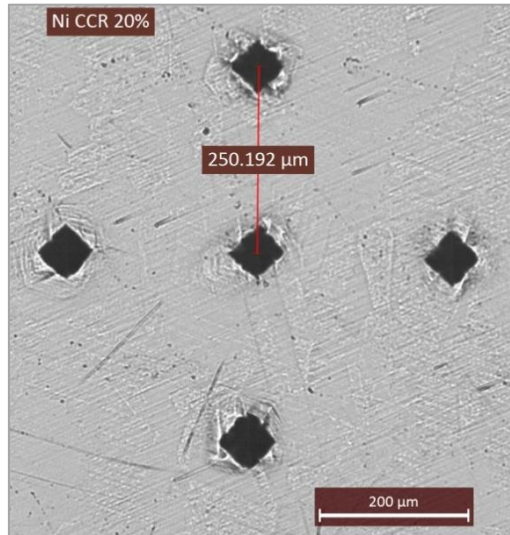
(b)

Figure 3.3.3: (a) Microindentation and (b) five microindentations at a gap of 250 µm in a CCR 20% sample taken during microhardness test.

Chapter 4

Experimental Results

4.1 Starting Material

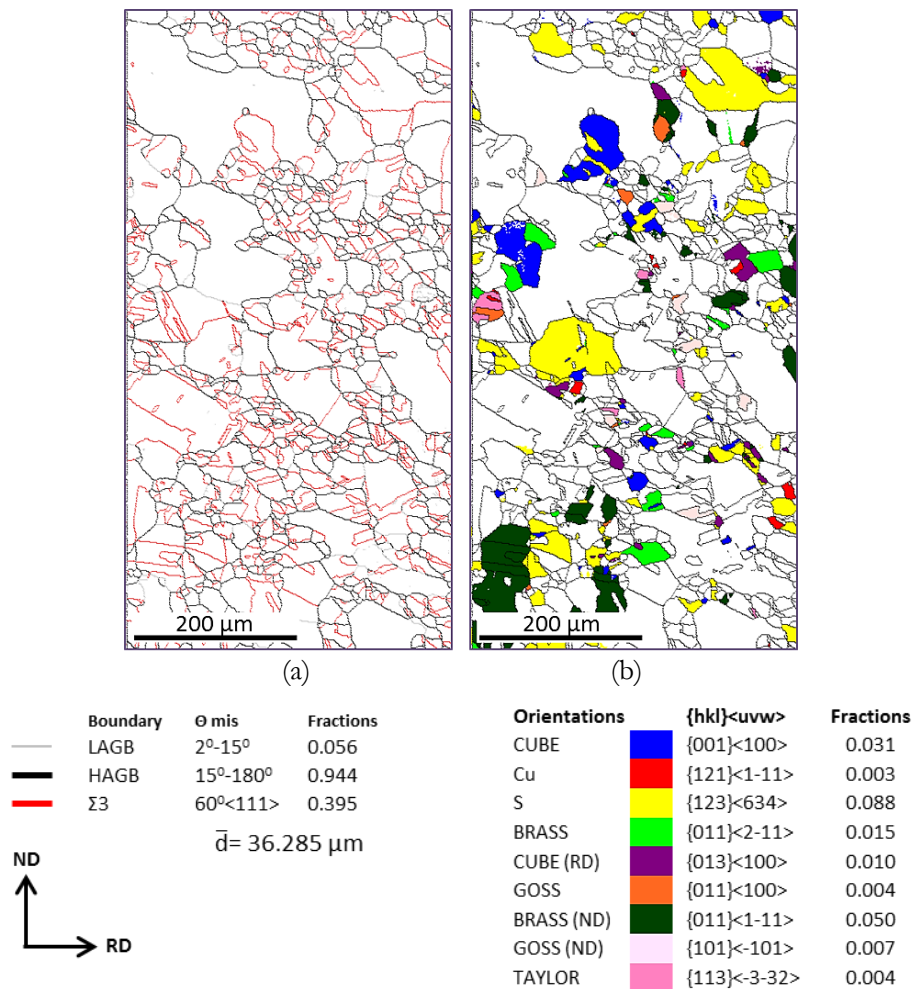| Boundary	Θ mis	Fractions
LAGB	2^0-15^0	0.056
HAGB	15^0-180^0	0.944
Σ3	60^0<111>	0.395

$\bar{d}$= 36.285 μm

ND
RD

Orientations	{hkl}<uvw>	Fractions
CUBE	{001}<100>	0.031
Cu	{121}<1-11>	0.003
S	{123}<634>	0.088
BRASS	{011}<2-11>	0.015
CUBE (RD)	{013}<100>	0.010
GOSS	{011}<100>	0.004
BRASS (ND)	{011}<1-11>	0.050
GOSS (ND)	{101}<-101>	0.007
TAYLOR	{113}<-3-32>	0.004

Figure 4.1.1: (a) GB and (b) GO maps of starting material

The Grain boundary (GB) map obtained from the EBSD scan of the RD-ND section of the Starting Material is shown by Fig. 4.1.1 (a). The Low Angle Grain Boundaries (LAGBs with misorientation angle (θ_{mis}); $15° \geq \theta_{mis} \geq 2°$) is shown by grey lines while the High Angle Grain Boundaries (HAGBs with $\theta_{mis}>15°$) are represented in black lines. The annealing twin

boundaries (Σ3 defined by 60°<111> relationship) are highlighted by red lines (The above conventions regarding grain boundaries are followed in all subsequent maps furnished in this section). The GB map reveals that the microstructure of starting material is fully recrystallized with the average grain size of ~36 μm (calculated by the intercept method). The high fraction of Σ3 boundaries indicates the large presence of annealing twins in the recrystallized microstructure. In the starting microstructure majority of the grains appear more or less uniform size but few relative large grains are also observed.

The corresponding GO map (Fig.4.1.1 (b)) shows the spatial distributions of standard orientations of rolling texture with their respective volume fractions. The color codes and notations of standard rolling texture components considered are summarized in Table 4.1. Evidently the starting material possesses weak texture probably due to the low deformation (~50% reduction in thickness) imparted before annealing. This is also clearly evidenced from the absence of intensities from the ideal location of standard rolling texture components in Fig. 4.1.2 (a) and 4.1.2(b) which shows the (111) pole figure (PF) and $\varphi_2=0°$, 45° and 65° sections of the orientation distribution function (ODF), respectively.

Table 4.1: Standard texture components considered during rolling of sheet materials.

Orientation	{ h k l }< u v w >	(φ_1, φ, φ_2)	Notations	Highlighting colour	
Cube	{001} <100>	(0°,0°,0°)	C	Blue	
Copper	{121} <1$\bar{1}$1>	(90°,35°,45°)	Cu	Red	
S	{123} <634>	(59°, 36.7°, 63.4°)	S	Yellow	
Brass	{011} <2$\bar{1}$1>	(35.3°, 45°, 0°)	Bs	Green	
Goss	{013} <100>	(45°,45°,0°)	G	Orange	
RD-Rotated Cube	{011} <100>	(0°,19°,0°)	C_{RD}	Purple	
ND-Rotated Brass	{011} <1$\bar{1}$1>	(54.7°,45°,0°)	Bs^{ND}	Dark green	
ND-Rotated Goss	{101} <$\bar{1}$01>	(90°,45°,90°)	G_{ND}	Light pink	
Taylor	{113} <$\bar{3}\bar{3}$2>	(90°,27°,45°)	T	Pink	
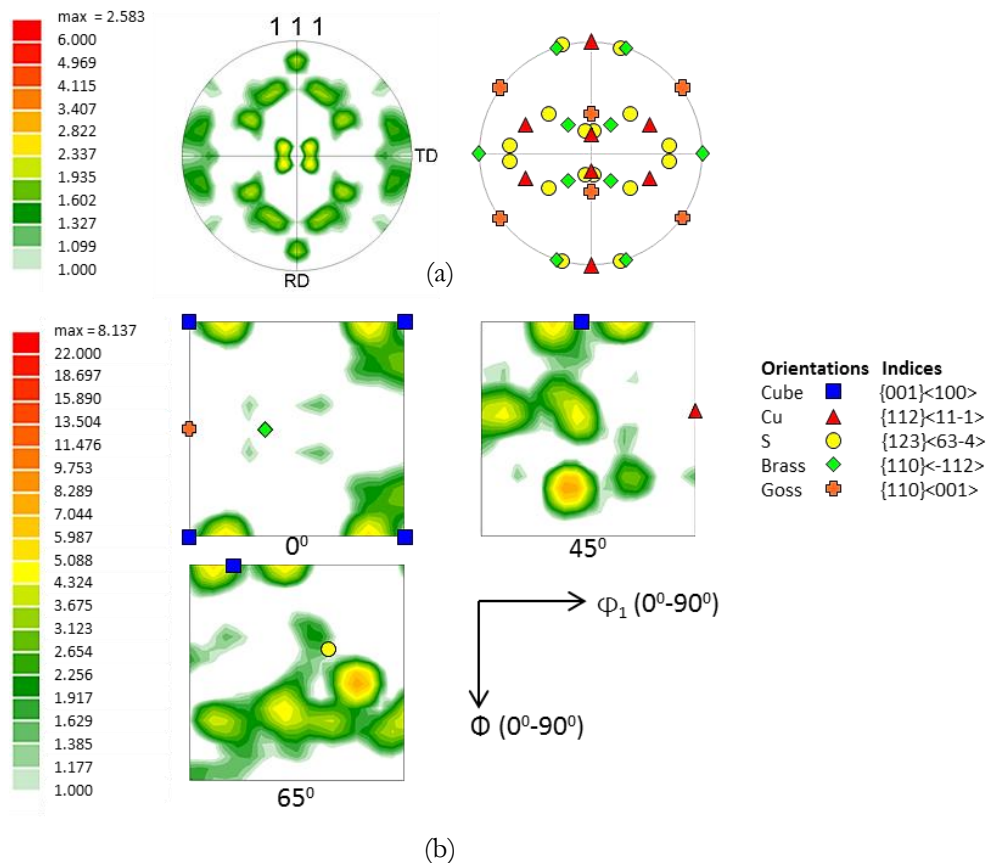
Figure 4.1.2: (a) Experimental (111) PF and (b) $\varphi_2=0°$, 45° and 65° sections of the ODF starting material. The ideal locations of standard rolling texture components have also been shown along with the PF and ODF sections.

4.2   Deformation by Straight cold rolling (SCR)

Boundary	Θ mis	Fractions
LAGB	2^0-15^0	0.728
HAGB	15^0-180^0	0.272
Σ3	60^0<111>	0.039

$\bar{d}$= 48.307 μm

Orientations	{hkl}<uvw>	Fractions
CUBE	{001}<100>	0.006
Cu	{121}<1-11>	0.033
S	{123}<634>	0.111
BRASS	{011}<2-11>	0.057
CUBE (RD)	{013}<100>	0.048
GOSS	{011}<100>	0.030
BRASS (ND)	{011}<1-11>	0.055
GOSS (ND)	{101}<-101>	0.022
TAYLOR	{113}<-3-32>	0.028

Figure 4.2.1: (a) GB and (b) GO maps of SCR processed 20% deformed Nickel sample

The GB map of 20% deformed SCR processed nickel is shown in Fig.4.2.1 (a). At this deformation level fraction of LAGBs in the microstructure is increased drastically to ~73%. The development of LAGB network at the interior of starting recrystallized grains indicates the development of a typical cell structure. The microstructure somewhat resembles the starting recrystallized microstructure but few grains appear slightly elongated along the rolling direction

(RD).The annealing twins are decreased with increasing deformation which is indicated by the reduced fraction of Σ3 CSL boundaries.

The corresponding Grain orientation (GO) map (Fig.4.2.1 (b)) reveals the presence of S, B_s and Bs^{ND} orientations possibly due to the presence of these orientations in the starting material. Figure 4.2.2(a) shows (111) PF which has detectable intensities at the ideal location of S and B_s which can be seen more clearly in the ODF sections of $\varphi_2=0°$ and 65° (Fig. 4.2.2 (b)) at the locations (59°, 36.7°, 63.4°) and (35.3°, 45°, 0°) corresponding to these two orientations.

Figure 4.2.2: (a) Experimental (111) PF and (b) φ2=0°, 45° and 65° sections of the ODF of 20% deformed SCR processed material. The ideal locations of standard rolling texture components have also been shown along with the PF and ODF sections.
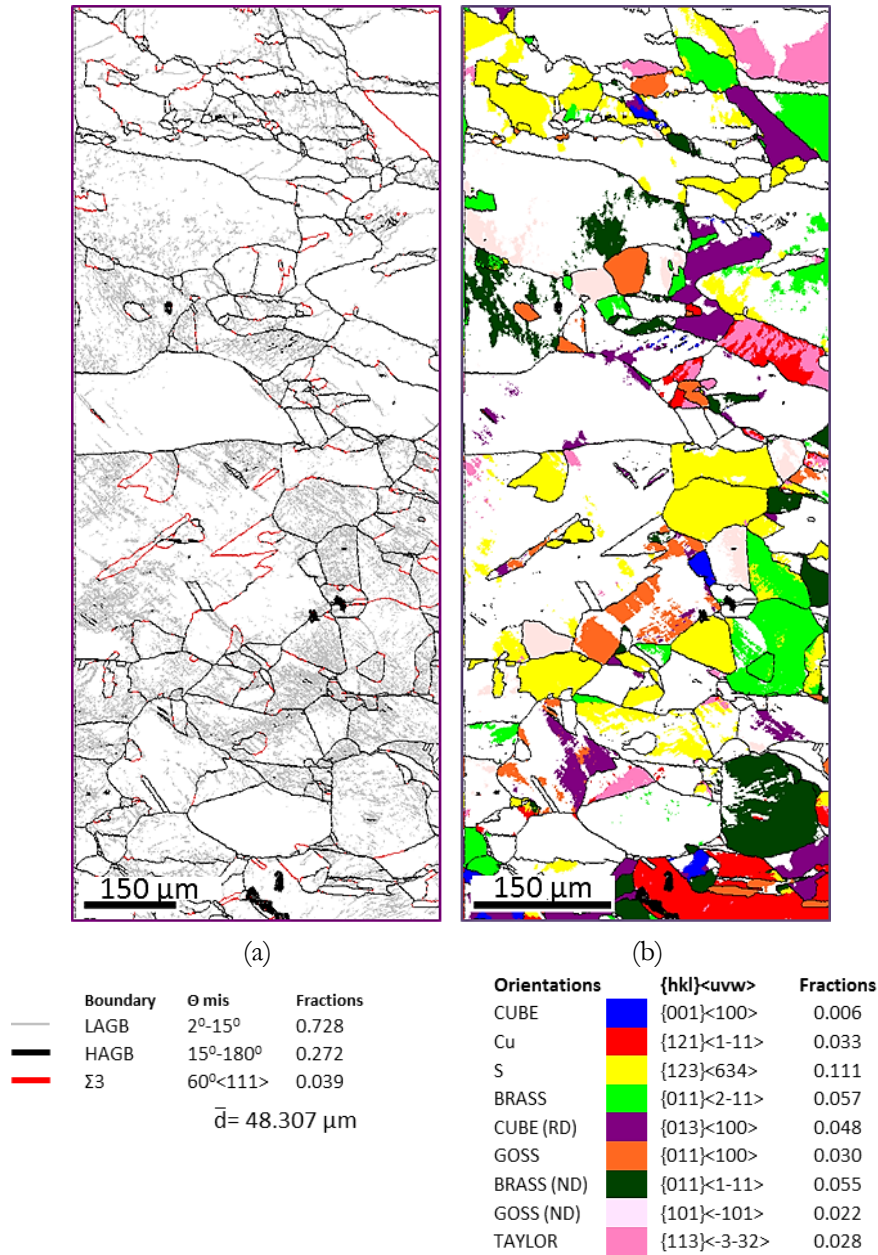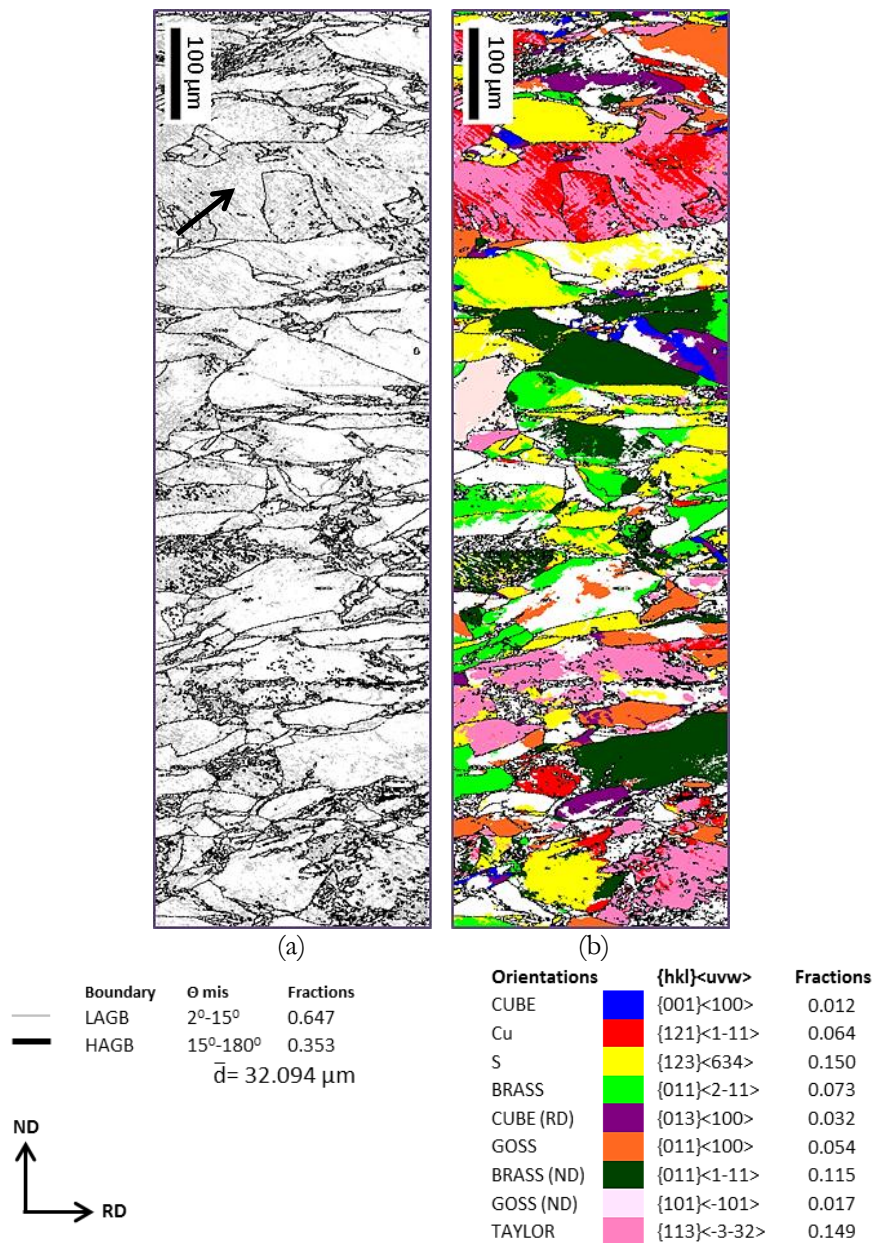
Figure 4.2.3: (a) GB and (b) GO maps of SCR processed 40% deformed Nickel sample

The GB map of 40% deformed SCR processed material is shown in Fig.4.2.3(a). There is slight decrease in LAGBs fraction (~64%) and corresponding increase in the HAGB fraction as compared to the 20% deformed material. The grains shape becomes more elongated along the RD.

After 40% reduction the rolling texture is enhanced as evidenced by the increase in the volume fractions of the S and Bs^{ND} components (Fig.4.2.3(b)). In the GO map it can be clearly observed that the spatial distribution of S and Bs is adjacent to each other. For Cu and T

orientations similar spatial distribution can be observed. Figure 4.2.4 (a) shows (111) PF which has relatively high intensity at ideal locations of S and Bs which is also corroborated from the $\varphi_2=0°$ and 65° ODF sections (Fig.4.2.4(b)).
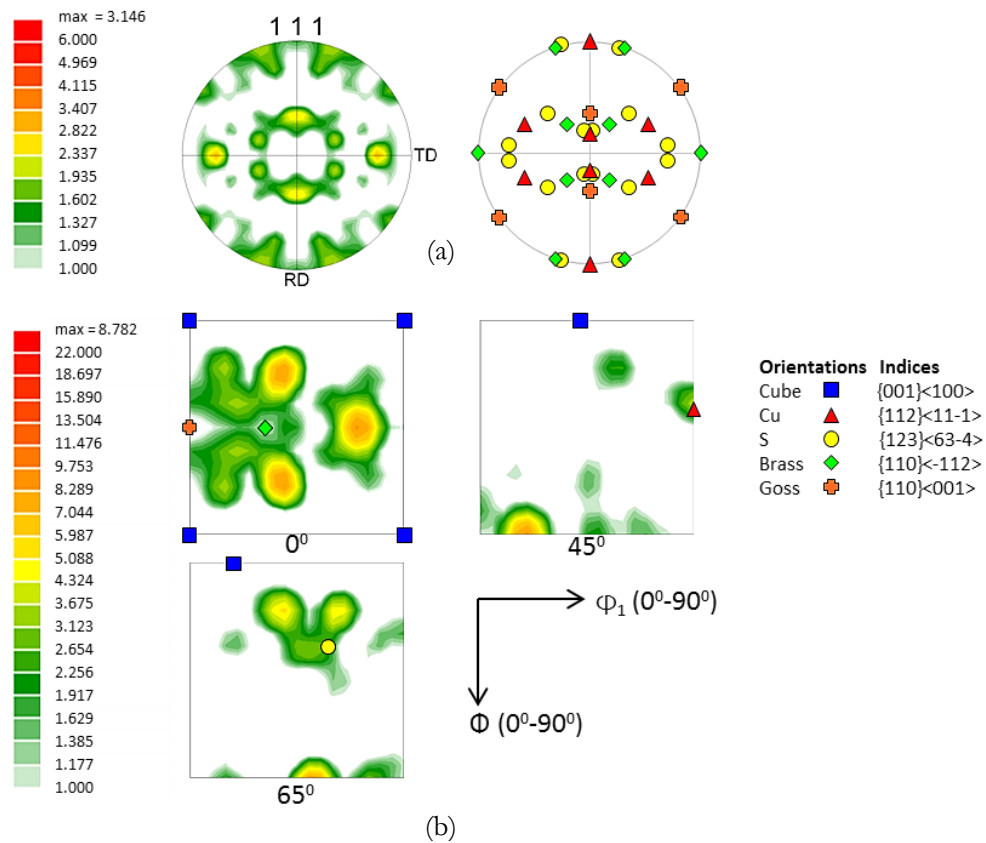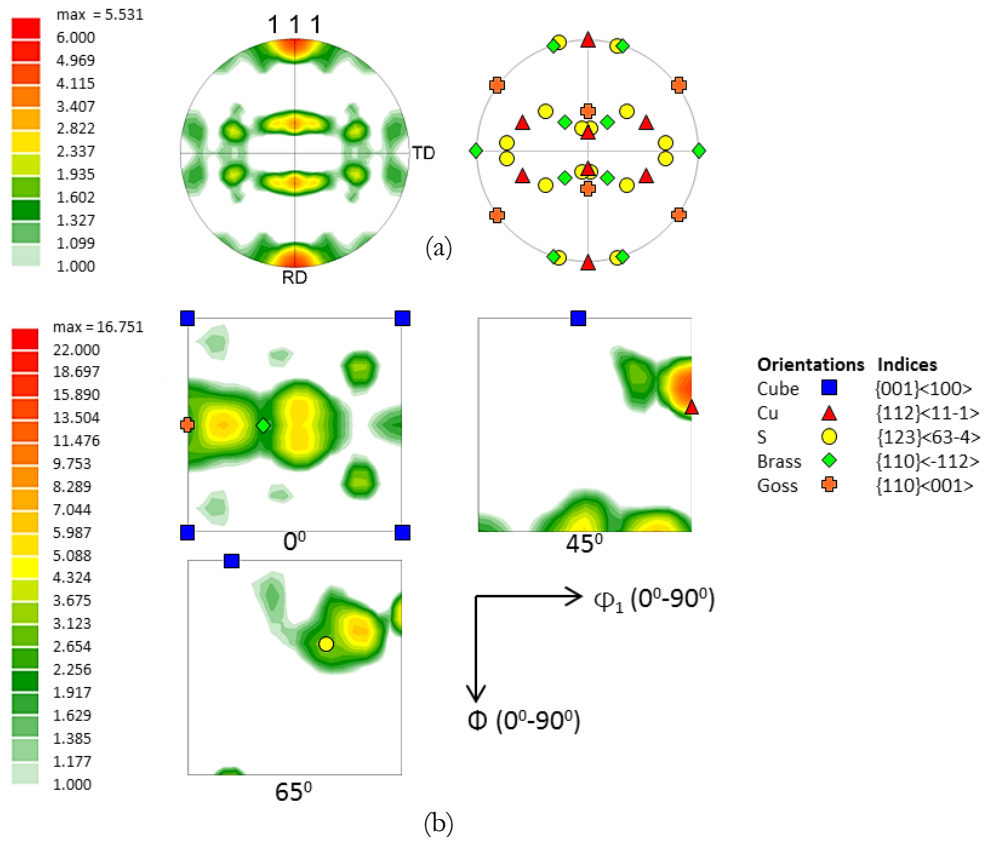

Figure 4.2.4: (a) Experimental (111) PF and (b) $\varphi_2=0°$, 45° and 65° sections of the ODF of 40% deformed SCR processed material. The ideal locations of standard rolling texture components have also been shown along with the PF and ODF sections.

Figure 4.2.5: (a) GB and (b) GO maps of SCR processed 65% deformed Nickel sample

The GB map (Fig.4.2.5(a)) of SCR processed Nickel sample after 65% deformation reveals the presence of banded lamellar microstructure. At 65% deformation grains are clearly elongated along the RD. This is a characteristic rolling microstructure generally for straight cold rolling route. There are no significant variations in fraction of LAGBs (~66%) and HAGBs (~34%) as compared to the 40% deformed material. But there is formation of microbands inside most of the grain presumably due to the generation and local rearrangement of dislocation structures.

These microbands are almost aligned at ~ 38°-45° with RD and these alignments are highlighted by black arrows in Fig.4.2.5 (a).

The corresponding GO map (Fig.4.2.5(b)) shows increased volume fraction of S (~24%), Bs (~9%), and Bs^{ND} (4%) components. At this strain level there is presence of significant amount of G orientation (~17%). In the microtexture it can be observed that in some locations the S & Bs and Cu & T orientation are adjacent to each other and sometimes present in the same band. The (111) PF (Fig.4.2.6(a)) shows the development of a typical pure metal or copper type texture. The (111) PF shows high intensities at ideal location of S and Bs. These ideal locations of S and Bs also overlap to some extent with the ideal Cu location in PF. Therefore, the intensities at these locations are combined intensities of all these orientations. In ODF sections (Fig.4.2.6(b)) intensity of these orientations can be viewed much clearly which shows increased intensities at the S, Bs and G locations.

Figure 4.2.6: : (a) Experimental (111) PF and (b) φ2=0°, 45° and 65° sections of the ODF of 65% deformed SCR processed material. The ideal locations of standard rolling texture components have also been shown along with the PF and ODF sections.
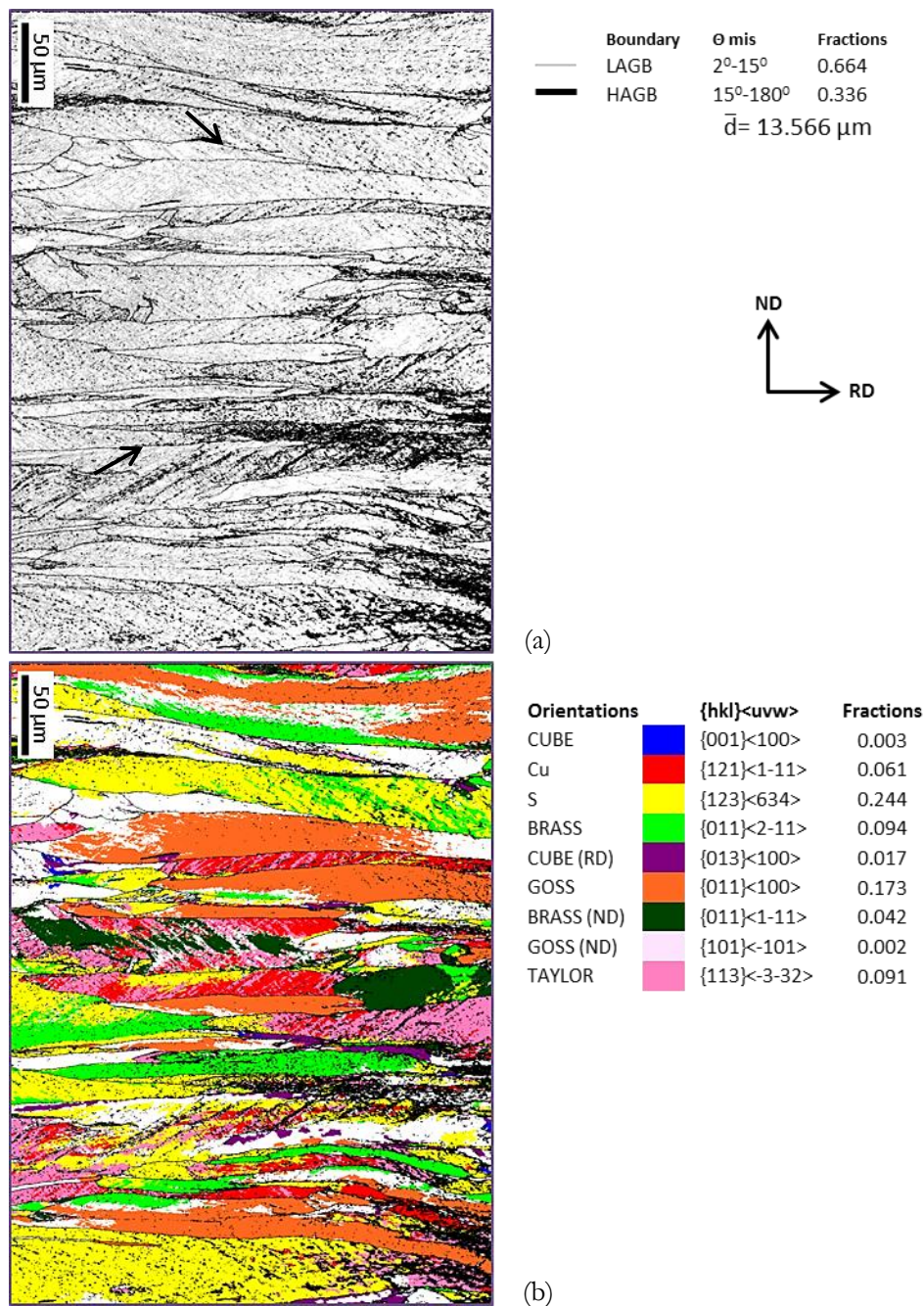
28
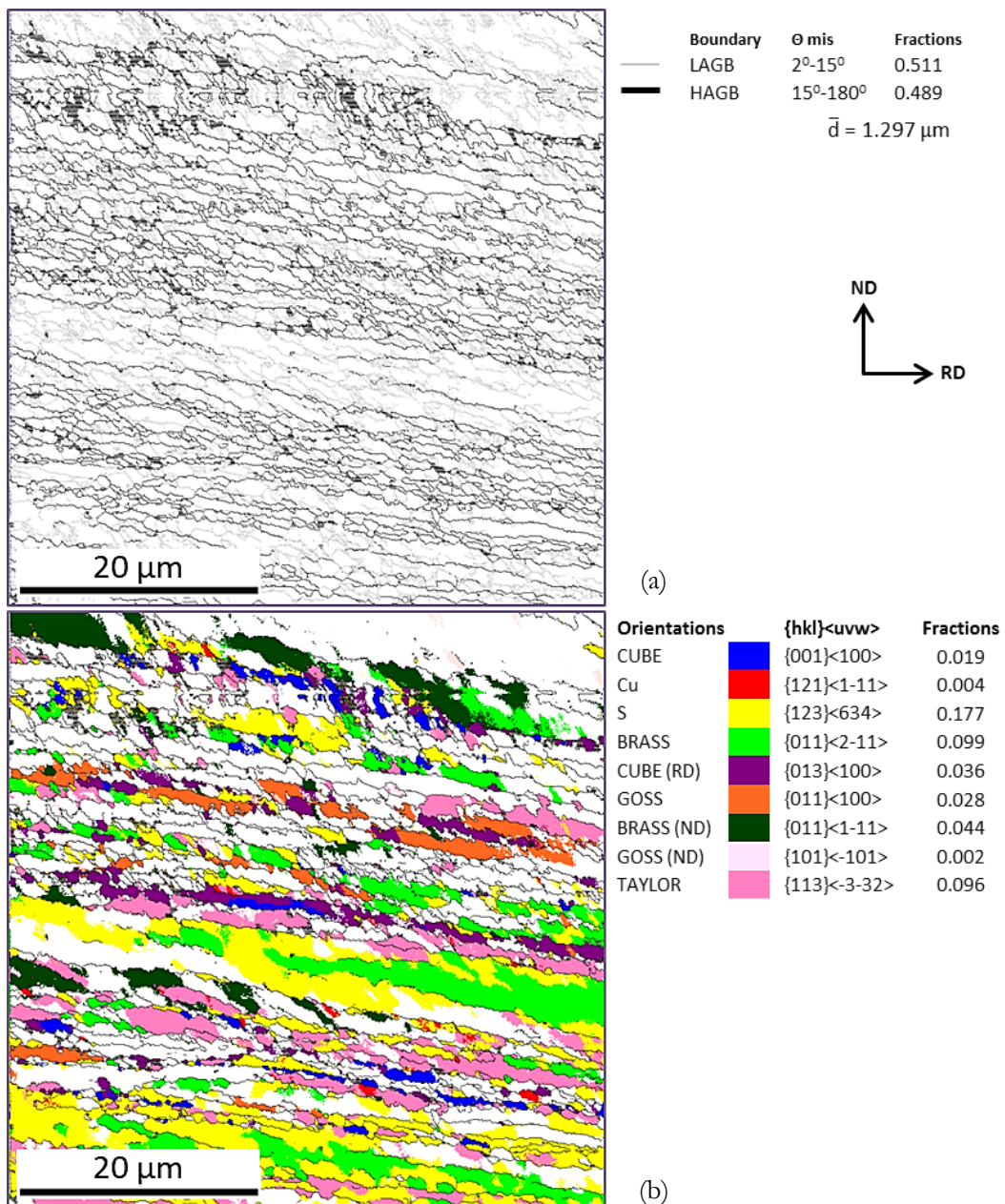
Figure 4.2.7: (a) GB and (b) GO maps of SCR processed 90% deformed Nickel sample

The GB map (Fig.4.2.7(a)) of SCR processed Nickel sample after 90% deformation shows very well developed lamellar microstructure typical of heavily deformed metals. The HAGB fraction increases further to 48% in this deformed condition.

The corresponding GO map (Fig.4.2.7 (b)) shows the microtexture after 90% deformation. It shows the dominant orientations in microtexture are S and Bs with ~17% and 9% respectively. The G orientation which was dominant at 65% deformation is significantly reduced (~3%

only). The S and Bs oriented bands are found to be adjacent to each other in the deformed microstructure. Interestingly, the (111) PF (Fig.4.2.8(a)) shows strong intensities around the S and Bs locations. The ODF sections (Fig.4.2.8(b)) also amply corroborate this observation.
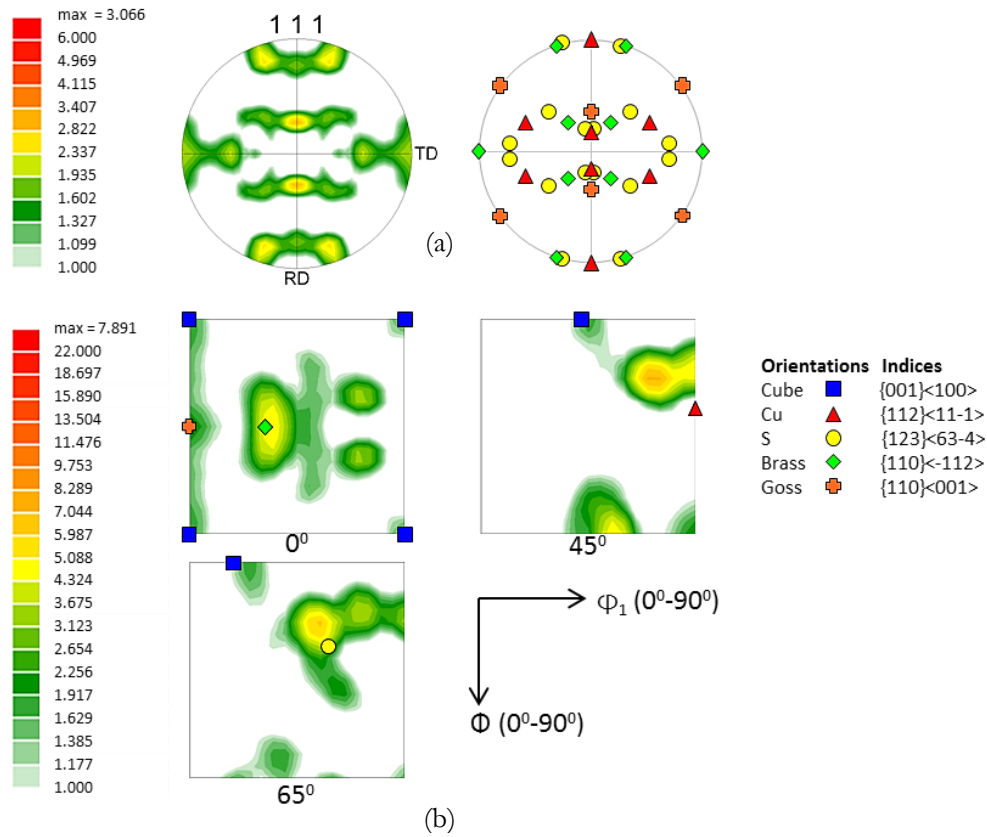
Figure 4.2.8: : (a) Experimental (111) PF and (b) φ2=0°, 45° and 65° sections of the ODF of 90% deformed SCR processed material. The ideal locations of standard rolling texture components have also been shown along with the PF and ODF sections.

Figure 4.2.9 represents the macrotexture of the SCR processed 90% deformed Nickel sample. These figures are obtained by the bulk texture measurement by X-ray diffraction.   The (111) PF (Fig.4.2.9(a)) shows the development of a typical rolling texture of heavily cold rolled medium to high SFE materials which is known as pure metal or copper type texture as already been introduced before.

The PF consists of all standard orientations except G. This is also substantiated from the ODF sections at φ2=0°, 45° and 65° (Fig.4.2.9 (a)) which clearly display the presence of S, Bs, and Cu components in the deformation texture. The macrotexture also shows the intensities at Cu orientations which were not present in the microtexture (Fig. 4.2.8).

.8   1.0   1.3   1.6   2.0
2.5   3.2   4.0   5.0   6.4

TD

RD

(a)

Orientations Indices
Cube   ■   {001}<100>
Cu   ▲   {112}<11-1>
S   ○   {123}<63-4>
Brass   ◆   {110}<-112>
Goss   ✛   {110}<001>

0^0

45^0

$\varphi_1\ (0^0\text{-}90^0)$

.50   1.50   4.50   8.50
12.0   16.0   22.0   30.0
38.0   44.0

$\Phi\ (0^0\text{-}90^0)$

65^0

(b)
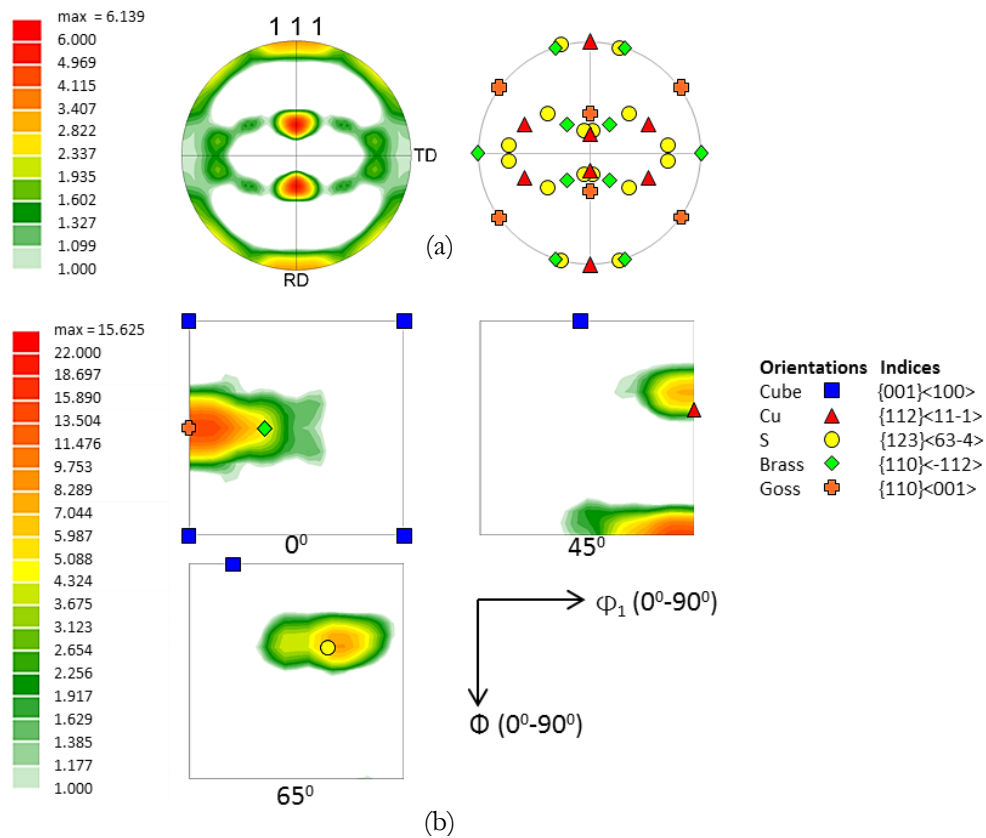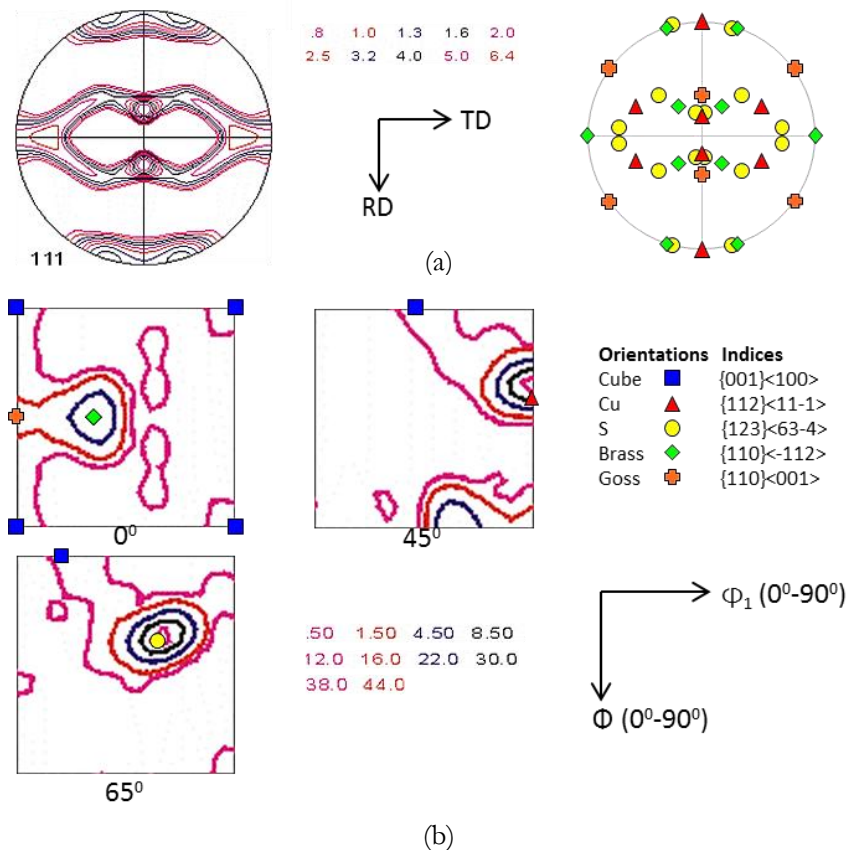
Figure 4.2.9: (a) Experimental (111) PF and (b) φ2=0°, 45° and 65° sections of the ODF of 90% deformed SCR processed material. The ideal locations of standard rolling texture components have also been shown along with the PF and ODF sections. These figures are obtained by the bulk texture measurement from X-Ray diffraction.

4.3 Deformation by Cross cold rolling (CCR)

The EBSD scan results of 20% deformed CCR processed Nickel sample is quite similar to the 20% SCR processed material. The similarity in the results is attributed to the identical rolling pass imparted in both the rolling routes. Therefore, the microstructure and microtexture of this deformed state are not given separately.

(a)   (b)

Boundary	Θ mis	Fractions
LAGB	2^0-15^0	0.887
HAGB	15^0-180^0	0.113
	$\bar{d}$= 43.315 μm	

ND
RD

Orientations		{hkl}<uvw>	Fractions
CUBE		{001}<100>	0.010
Cu		{121}<1-11>	0.000
S		{123}<634>	0.001
BRASS		{011}<2-11>	0.002
CUBE (RD)		{013}<100>	0.010
GOSS		{011}<100>	0.000
BRASS (ND)		{011}<1-11>	0.003
GOSS (ND)		{101}<-101>	0.039
TAYLOR		{113}<-3-32>	0.000

Figure 4.3.1: (a) GB and (b) GO maps of CCR processed 40% deformed Nickel sample

The GB map of 40% deformed CCR processed Nickel sample is shown in Fig.4.3.1(a). It shows some elongated grains toward Normal direction (ND) conceivably due to the variation in the grains shape of few in deformed structure due to the change in rolling directions in consecutive passes. There are microbands introduced in the microstructure which are aligned at ~40°.

Interestingly, the corresponding GO map (Fig.4.3.1(b)) shows that grains have no typical rolling texture orientations. Each standard orientation have volume fraction less than 3%. Some microbands possess C and C_{RD} orientations .It is also confirmed by the (111) PF & ODF sections (Fig.4.3.2 (a) & (b)) in which all intensities are skipped from ideal positions of standard orientations. Consequently, the 40% CCR processed Nickel shows very weak rolling texture.
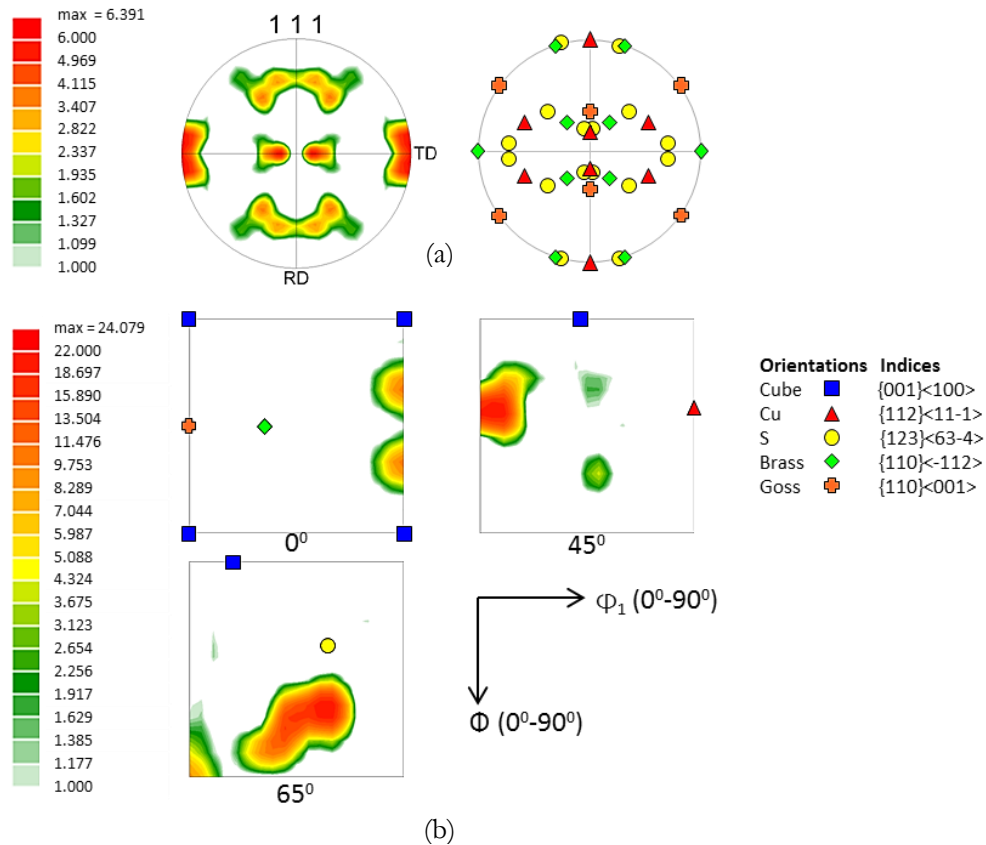
Figure 4.3.2: : (a) Experimental (111) PF and (b) φ2=0°, 45° and 65° sections of the ODF of 40% deformed CCR processed material. The ideal locations of standard rolling texture components have also been shown along with the PF and ODF sections.

Boundary	Θ mis	Fractions
LAGB	2^0-15^0	0.717
HAGB	15^0-180^0	0.283

$\bar{d}$= 5.949 µm

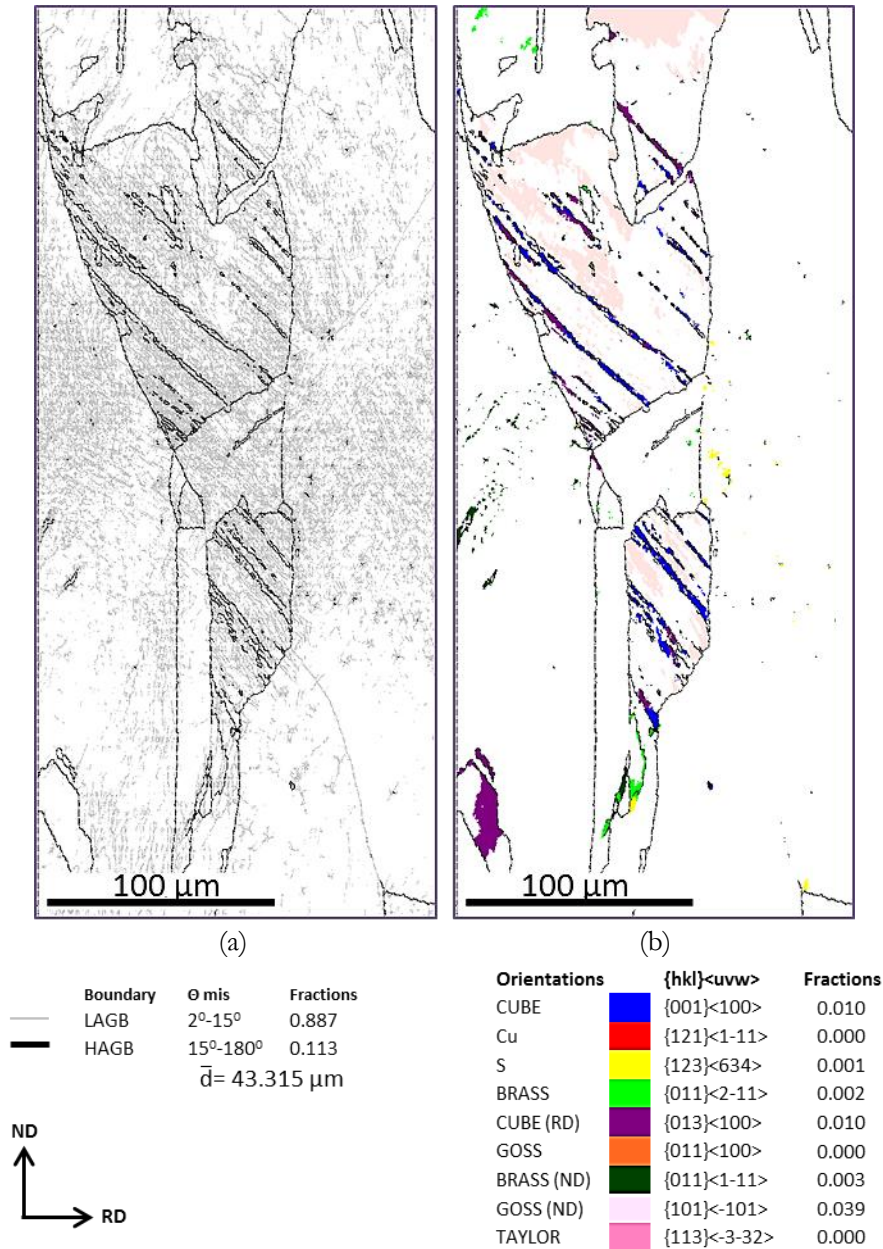| Orientations	{hkl}<uvw>	Fractions
CUBE	{001}<100>	0.052
Cu	{121}<1-11>	0.006
S	{123}<634>	0.098
BRASS	{011}<2-11>	0.030
CUBE (RD)	{013}<100>	0.056
GOSS	{011}<100>	0.012
BRASS (ND)	{011}<1-11>	0.038
GOSS (ND)	{101}<-101>	0.053
TAYLOR	{113}<-3-32>	0.001

Figure 4.3.3: (a) GB and (b) GO maps of CCR processed 65% deformed Nickel sample

The GB map (Fig.4.3.3(a)) of 65% CCR processed Nickel sample shows fragmented microstructure with no apparent microbands. This microstructure is possibly formed due to the rotations of sub-structure caused by the change in rolling direction by 90°.

The GO map (Fig.4.3.3 (b)) shows S, C, and C_{RD} as dominant texture components. In the microtexture the S, Bs. C and C_{RD} oriented regions appear to be fragmented and isolated by randomly oriented regions highlighted by white color. (111) PF (Fig.4.3.4(a)) shows weak

intensities at the ideal location of S and Bs, which is also evidenced in the relevant ODF sections (Fig.4.3.4(b).

Figure 4.3.4: (a) Experimental (111) PF and (b) φ2=0°, 45° and 65° sections of the ODF of 65% deformed CCR processed material. The ideal locations of standard rolling texture components have also been shown along with the PF and ODF sections.
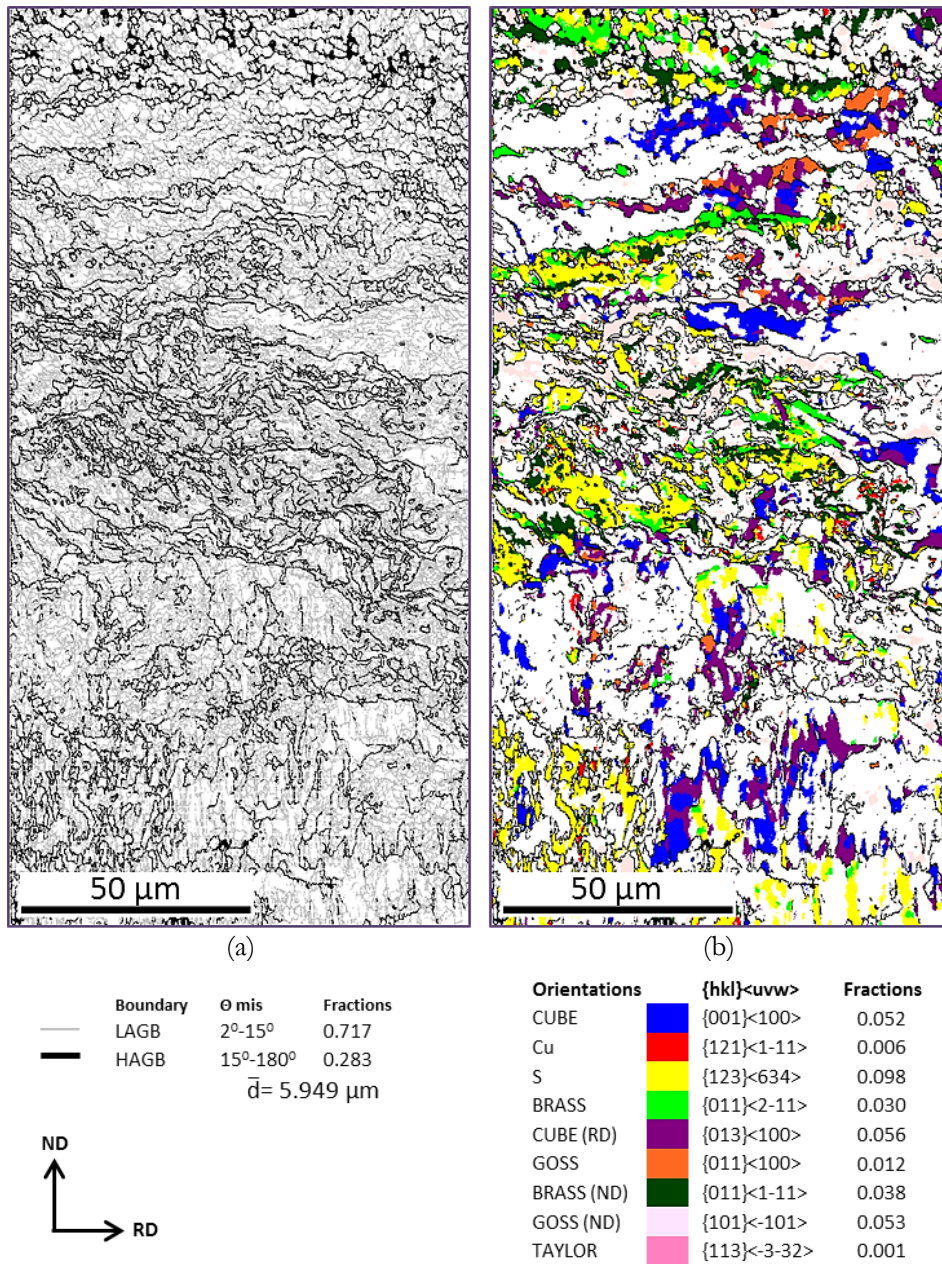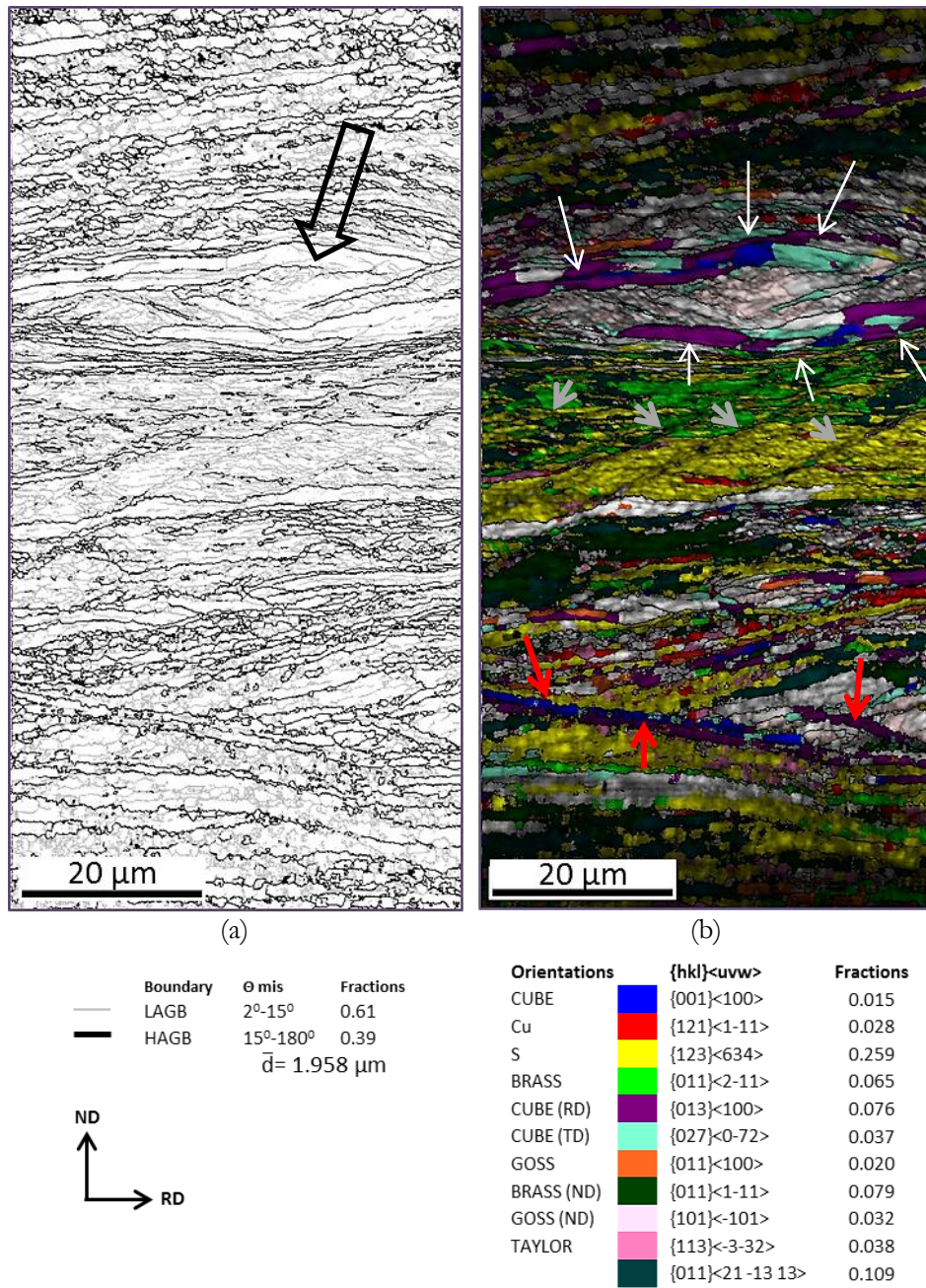
Figure 4.3.5: (a) GB (b) GO maps of CCR processed 90% deformed Nickel sample

The GB Map (Fig.4.3.5(a)) shows ultrafine structure sub-divided by HAGBs. Remarkably, the deformed structure consists of intense locally sheared regions indicated by block arrow. Inside this locally sheared region a long cube band indicated by thin white arrows could be clearly observed. The orientation inside the band changes continuously from C_{RD} from one end of the band to C_{TD} orientation at the other end. Very clear intersecting shear bands indicated by grey arrows could be easily observed in the microstructure. Interestingly, few of the shear bands

indicated by red arrows have C or C_{RD} orientations. Overall the dominant orientations observed are the S, Bs and Bs^{ND} components including $\{011\}<21\ \overline{13}\ 13>$. The (111) PF (Fig.4.3.6(a)) and the relevant ODF sections (Fig.4.3.6(b)) amply show the development of strong B_S and B_S^{ND} components. This is consistently observed for EBSD maps taken from other regions of the CCR processed material (Fig. 4.3.7).

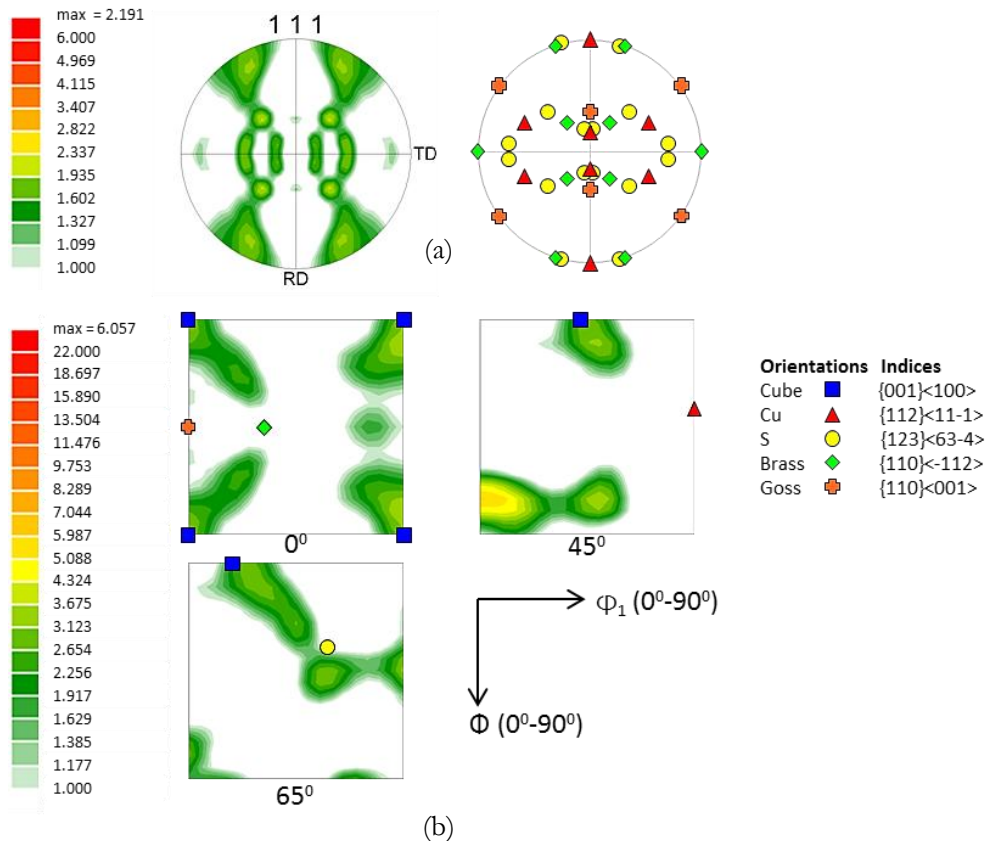
Figure 4.3.6: (a) Experimental (111) PF and (b) φ2=0°, 45° and 65° sections of the ODF of 90% deformed CCR processed material. The ideal locations of standard rolling texture components have also been shown along with the PF and ODF sections.

Orientations	{hkl}<uvw>		Fractions
CUBE	{001}<100>	(blue)	0.012
Cu	{121}<1-11>	(red)	0.031
S	{123}<634>	(yellow)	0.163
BRASS	{011}<2-11>	(green)	0.190
CUBE (RD)	{013}<100>	(purple)	0.018
CUBE (TD)	{027}<0-72>	(cyan)	0.009
GOSS	{011}<100>	(orange)	0.008
BRASS (ND)	{011}<1-11>	(dark green)	0.116
GOSS (ND)	{101}<-101>	(light pink)	0.002
TAYLOR	{113}<-3-32>	(pink)	0.032
	{011}<21 -13 13>	(dark teal)	0.238

Figure 4.3.7: GO maps of CCR processed 90% deformed Nickel sample taken from EBSD Scan of another region.

The deformation of CCR processed 90% deformed Nickel sample was further studied by X-ray diffraction methods. The (111) PF (Fig.4.3.8(a)) and the relevant ODF sections (Fig.4.3.7(b)) shows the maximum intensity at the S and Bs locations. The intensity maximum associated with the B_S orientation is actually found to be at the location $(\varphi_1,\varphi,\varphi_2) = (41.3°,45°,0°)$ corresponding to the orientation $\{011\}<21\,\overline{13}13>$. For this reason this orientation has already been included in the orientation maps of 90% deformed CCR processed material shown previously (Figures 4.3.6 and 4.3.7).

It may be noted that both microtexture and macrotexture results of heavily deformed CCR processed material indicate the development of strong B_S and $B_S{}^{ND}$ components and are thus found to be in excellent agreement with each other.
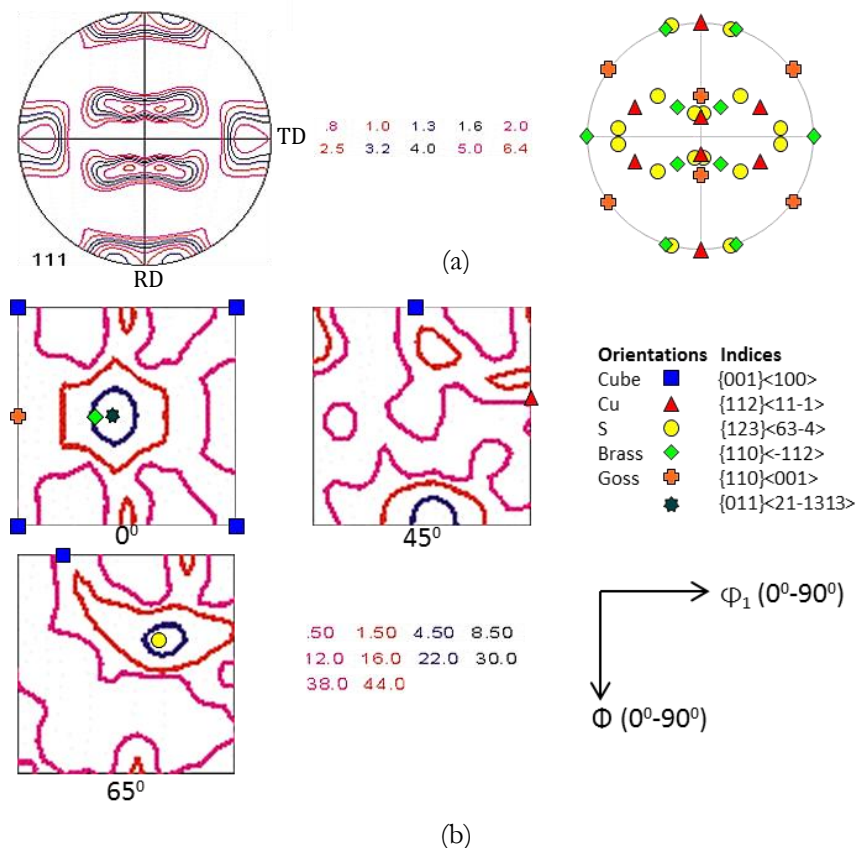
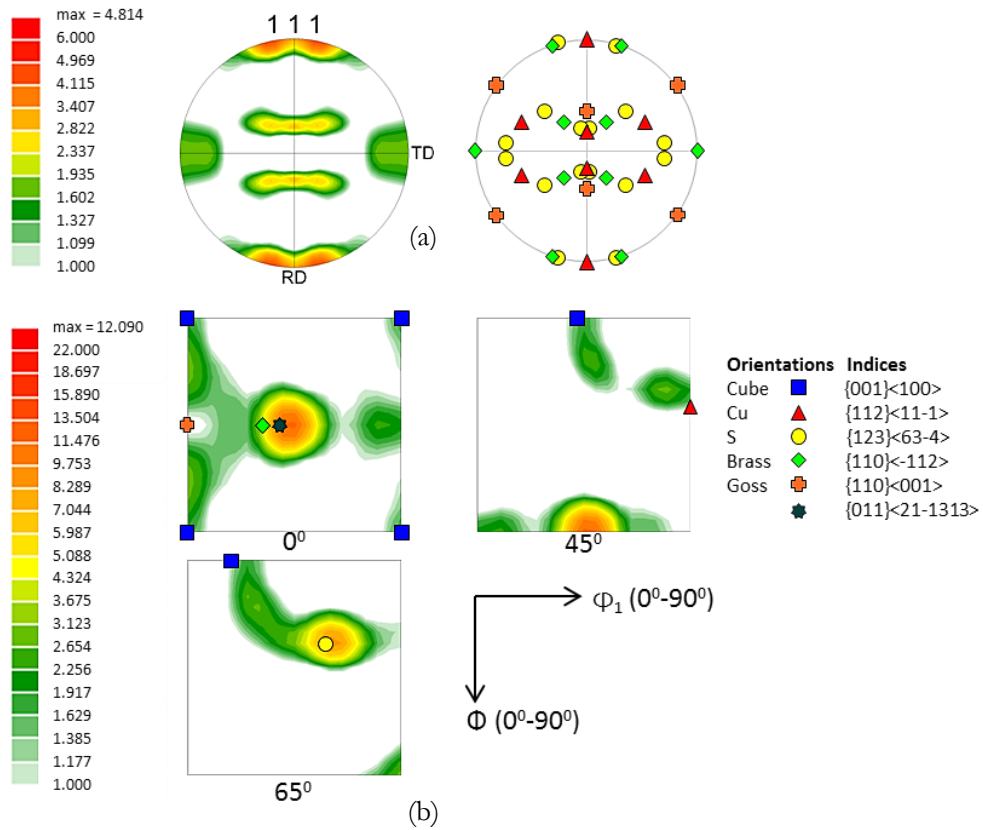

Figure 4.3.8: (a) Experimental (111) PF and (b) φ2=0°, 45° and 65° sections of the ODF of 90% deformed CCR processed material. The ideal locations of standard rolling texture components have also b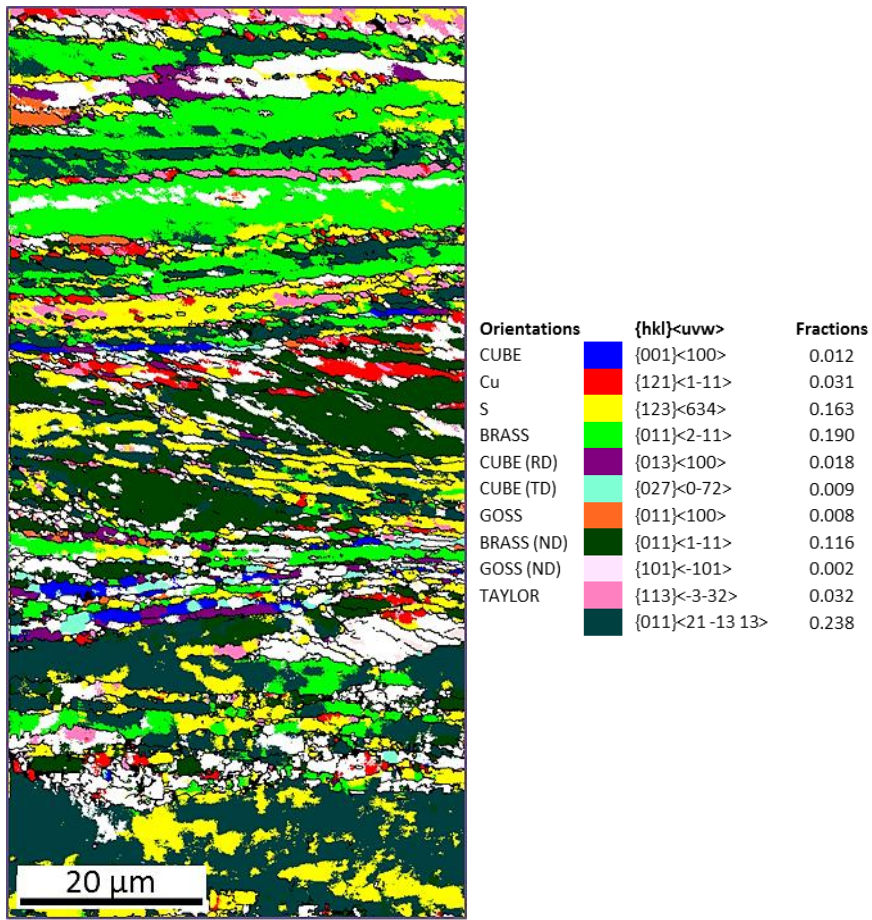een shown along with the PF and ODF sections. These figures are obtained by the bulk texture measurement from X-Ray diffraction.

4.4 Evolution of Mechanical properties with deformation (Hardness)

The evolution of mechanical properties with deformation and rolling route is determined by hardness testing. The change in hardness with deformation for both rolling route is shown in Fig.4.4.1. It can be observed that hardness value (on HV scale) increases with increasing deformation in both cases. SCR and CCR processed materials show very similar hardness values at all deformation level. The hardness of CCR processed material is found to be slightly more than its SCR processed counterpart after 90% deformation.
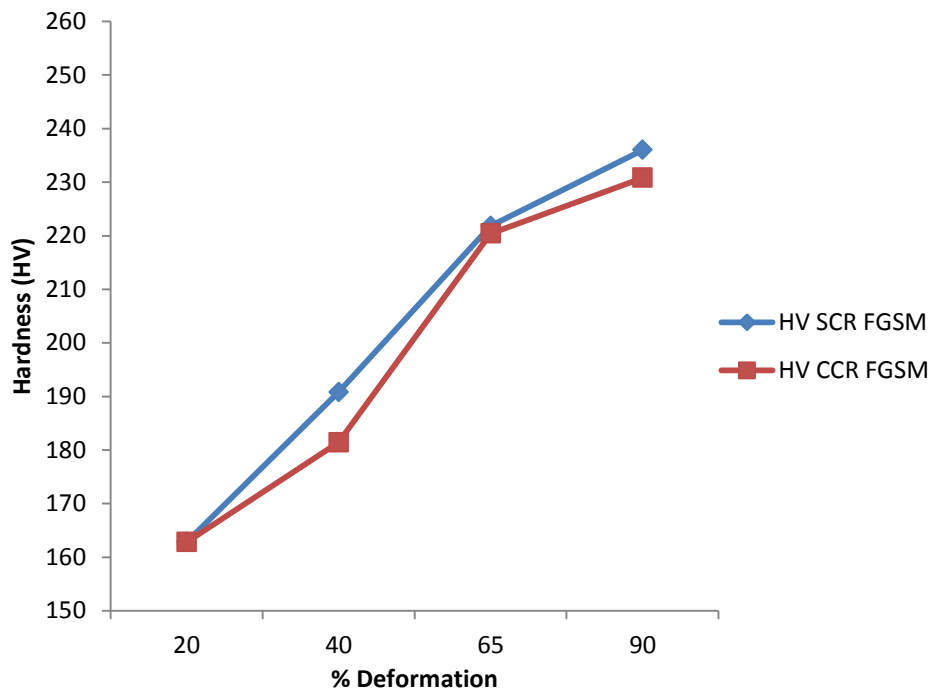
Figure 4.4.1: Change in hardness with %deformation (strain) in nickel processed by SCR and CCR routes

4.5 Recrystallization texture

Evolution of recrystallization texture in SCR processed high purity Nickel has been studied extensively [12,13]. It has been widely reported that the recrystallization texture is predominantly a cube texture (Fig 4.5.1). On the basis of these previous research results, in the present study further analysis of the recrystallization texture of 90% SCR processed material is not carried out.
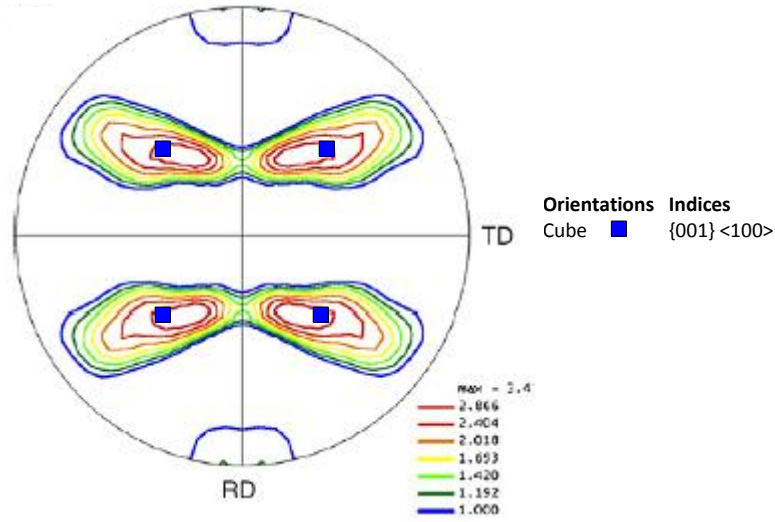
Figure 4.5.1: Experimental (111) PF (by EBSD scan) with ideal location of Cube orientation (shown by blue box) of SCR processed and subsequent annealed pure Nickel sample at 500°C [13]

Table 4.5: Standard orientations considered in the recrystallization texture of annealed nickel samples in addition to standard orientations of deformation texture.

Orientation	{ h k l }< u v w >	$(\varphi_1, \varphi, \varphi_2)$	Notations	Highlighting colour	
TD -Rotated Cube	{027} <0$\bar{7}$2>	(90°, 15.95°, 0°)	C_{TD}	Aqua	
Cube (Twinned)	{221} <1$\bar{2}$2>	(45°, 70.53°, 45°)	C^T	Light Grey	
RD-Rotated Cube (Twinned)	{185} <21$\bar{2}$>	(42.1°, 83.9°, 58°)	C_{RD}^T	Dark Red	
TD-Rotated Cube (Twinned)	{445} <13$\overline{23}$8>	(22.8°, 48.52°, 45°)	C_{TD}^T	Light Blue	
ND fiber orientation	{111}<1$\bar{1}$0>	(0°, 55°, 45°)	-	Olive Green	

Recrystallization texture of nickel following 90% deformation by CCR route and subsequently annealed at 400°C for 1 hr is shown in Fig.4.5.2. Remarkably, the (111) PF shows the development of ND||<111> fiber texture which is quite unusual as far as recrystallization texture of conventionally deformed medium to high stacking fault energy materials are concerned. Since such an ND fiber texture will be clearly visible in the corresponding φ_2= 45° section of the ODF, this particular section is shown separately (Fig.4.5.2(b)). The φ_2= 45° section shows that intensities along the fiber is not homogenously distributed with local intensity maximum at the location (0°, 55°, 45°) (shown by star) for {111}<1$\bar{1}$0> and (23°, 49°, 45°) (shown by inverted triangle) for {445} <13$\overline{23}$8> orientations.

The corresponding GO map shows the spatial distribution of orientations along with the above two recrystallization texture components (Fig 4.5.3(b)). The map shows the ND||<111> fiber texture component {111}<1$\bar{1}$0> shown by olive green and {445} <13$\bar{2}\bar{3}$8> highlighted by light blue have volume fraction of ~10% and 12% respectively. The volume fraction of the C component is quite small but the presence of the C_{TD} component is noticed having volume fraction of ~6.2%. Interestingly, in the GO map the orientations (aqua) is found mostly adjacent to fiber orientation {445} <13$\bar{2}\bar{3}$8> separated by Σ3 annealing twin boundaries (highlighted by red line) indicating that this fiber orientation is twin related orientation of C_{TD} and designated by $C_{TD}{}^T$. The dominant orientation of deformation texture Bs and BsND has been reduced drastically to below 3.5% after annealing.
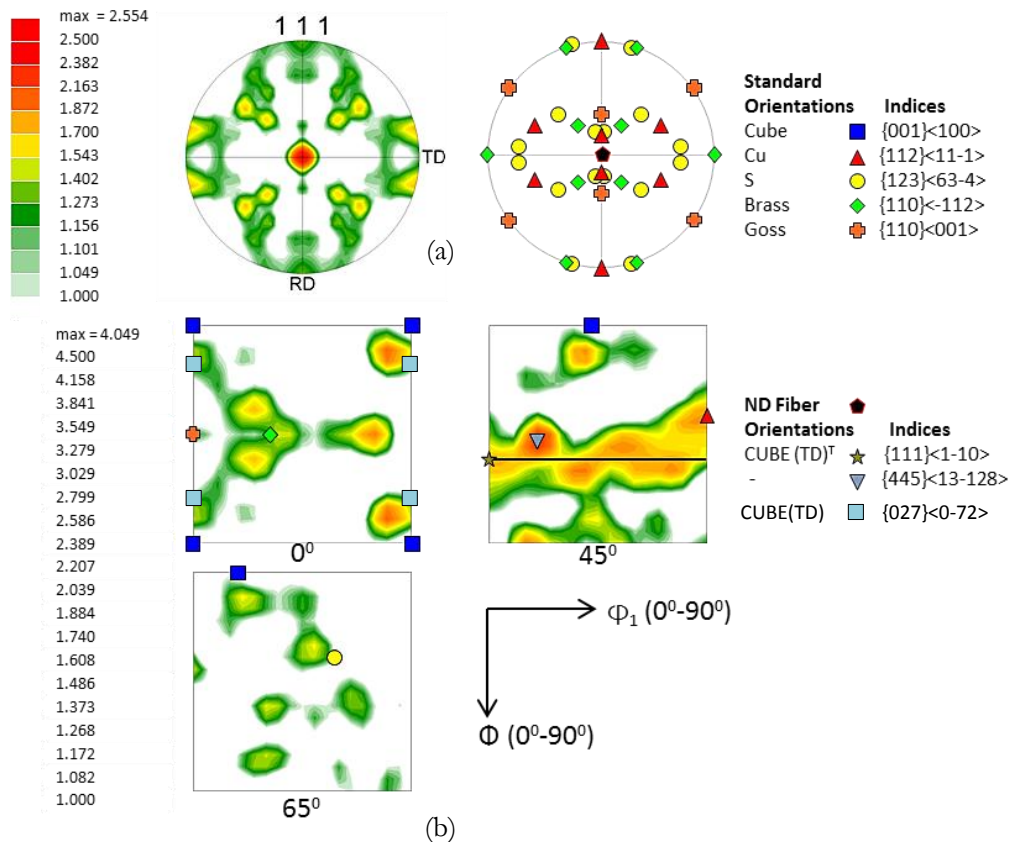

Figure 4.5.2: (a) Experimental (111) PF and (b) φ2=0°, 45° and 65° sections of the ODF of 90% deformed CCR processed and subsequently annealed (at 400°C for 1 hr.) Nickel sample. The ideal locations of orientations considered have also been shown along with the PF and ODF sections.

Boundary	Θ mis	Fractions
LAGB	2°-15°	0.033
HAGB	15°-180°	0.967
Σ3	60°<111>	0.398

$\bar{d} = 26\ \mu m$

Orientations	{hkl}<uvw>	Fractions
CUBE	{001}<100>	0.017
Cu	{121}<1-11>	0.044
S	{123}<634>	0.063
BRASS	{011}<2-11>	0.047
CUBE (RD)	{013}<100>	0.018
GOSS	{011}<100>	0.012
BRASS (ND)	{011}<1-11>	0.029
GOSS (ND)	{101}<-101>	0.008
TAYLOR	{113}<-3-32>	0.017
CUBE(TD)	{027}<0-72>	0.062
CUBE^T	{221}<1-22>	0.051
CUBE (RD)^T	{185}<21-2>	0.048
CUBE(TD)^T	{445}<13-23 8>	0.121
ND FIBRE ORIENTATION	{111}<1-10>	0.093

Figure 4.5.3: (a) GB (b) GO maps of Nickel sample which is CCR processed 90% deformed and subsequently annealed at 400°C

Recrystallization texture of following annealing at 800°C for 1 hr. is shown in Fig.4.5.5. The GO map (Fig 4.5.4(b)) shows few large C_{TD} oriented grains. The volume fraction of C_{TD} orientation although increases in comparison to the 400°C but still is rather low (~14%) as compared to the 400°C material. The presence of the C_{TD} orientation is corroborated from the corresponding (111) PF (Fig.4.5.5(a)) and $\varphi_2=0°$ section of the ODF (Fig.4.5.5(b)). The fiber observed in the 400°C annealed specimen becomes weaker which may be clearly understood by comparing the intensities of the contours of around the central location of (111) PF of the 800°C (Fig.4.5.5(a)) and the $\varphi_2=45°$ section (Fig.4.5.5(b)) with those of the 400°C (Fig.4.5.2)

43

specimen. The two fiber orientations observed in the 400°C annealed specimen i.e. ($(111)[1\overline{1}0]$ and $(445)[13\overline{2}\overline{3}8]$) are decreased after annealing at 800°C and their volume fractions are ~1.6% and 8%, respectively. Significant presence of the S orientation (~16%) could also be observed.

Boundary	Θ mis	Fractions
LAGB	2⁰-15⁰	0.306
HAGB	15⁰-180⁰	0.694
Σ3	60⁰<111>	0.285

$\bar{d}$ =112 µm

200 µm (a)

Orientations	{hkl}<uvw>	Fractions
CUBE	{001}<100>	0.011
Cu	{121}<1-11>	0.082
S	{123}<634>	0.064
BRASS	{011}<2-11>	0.016
CUBE (RD)	{013}<100>	0.089
GOSS	{011}<100>	0.019
BRASS (ND)	{011}<1-11>	0.042
GOSS (ND)	{101}<-101>	0.002
TAYLOR	{113}<-3-32>	0.044
CUBE(TD)	{027}<0-72>	0.146
CUBE ᵀ	{221}<1-22>	0.083
CUBE (RD) ᵀ	{185}<21-2>	0.047
CUBE(TD) ᵀ	{445}<13-23 8>	0.085
ND FIBRE ORIENTATION	{111}<1-10>	0.016

200 µm (b)

Figure 4.5.4: (a) GB (b) GO maps of Nickel sample which is CCR processed 90% deformed and subsequently annealed at 800°C

44

Figure 4.5.5: (a) Experimental (111) PF and (b) φ2=0°, 45° and 65° sections of the ODF of 90% deformed CCR processed and subsequently annealed (at 800°C for 1 hr.) Nickel sample. The ideal locations of orientations considered have also been shown along with the PF and ODF

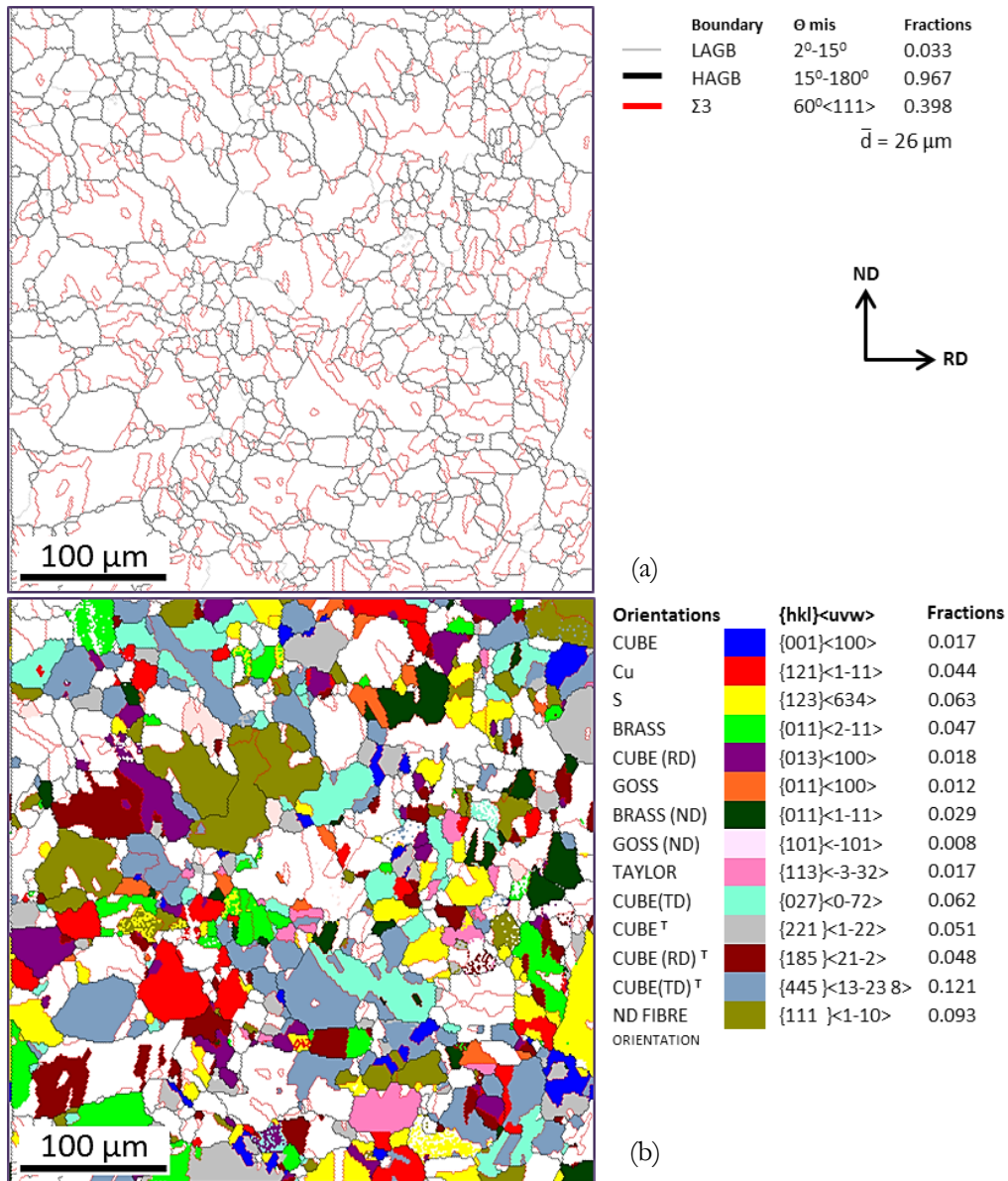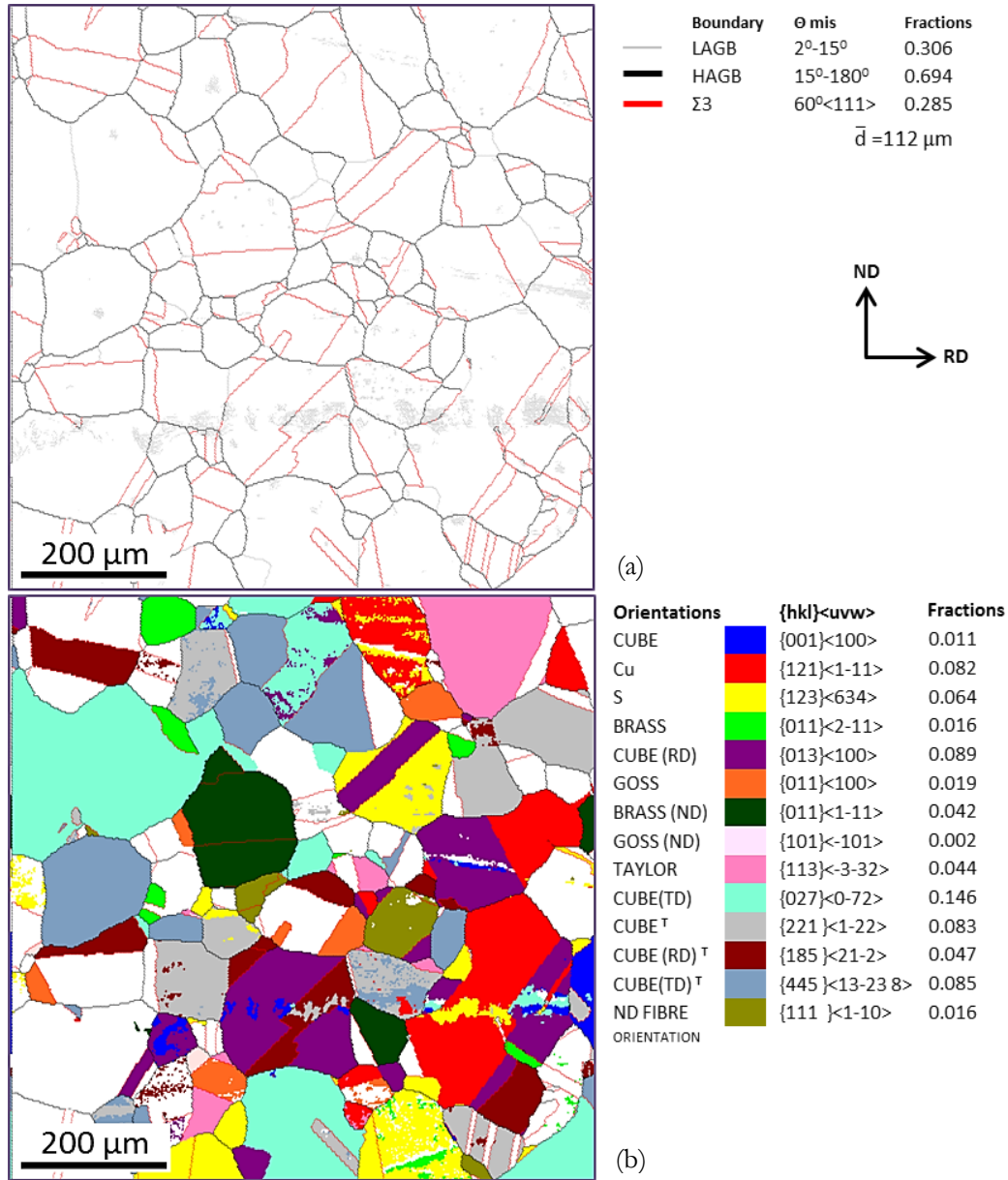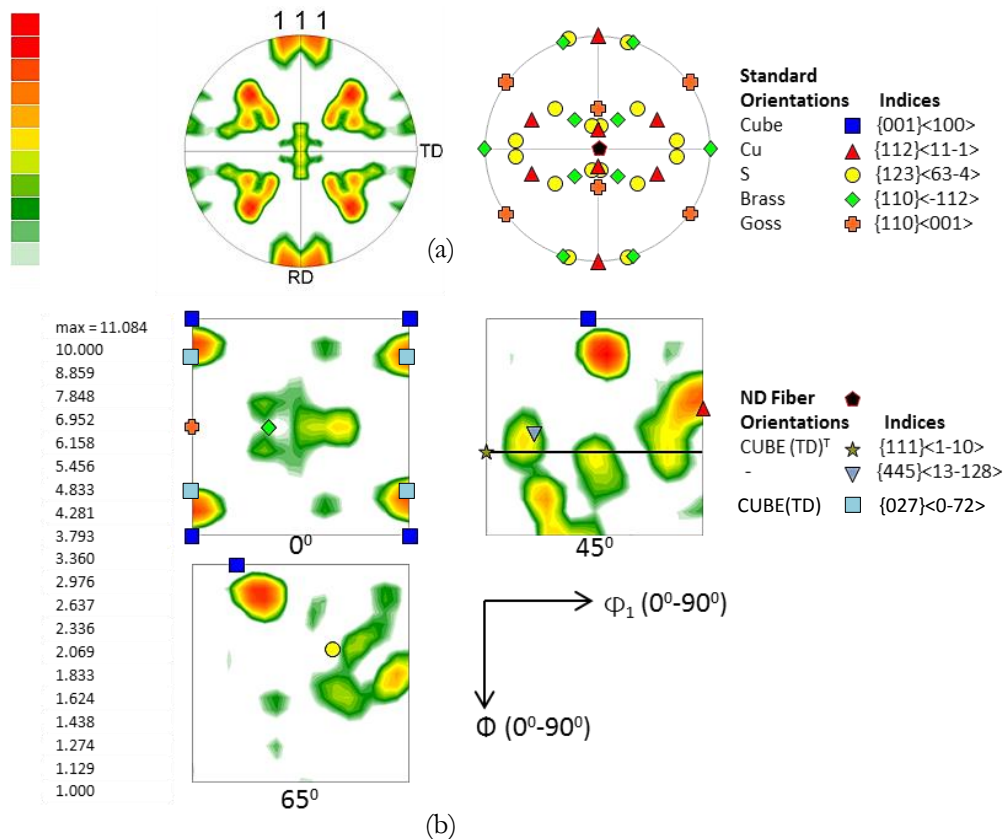Figure 4.5.6(a) and (b) show the GB and coincidence site lattice (CSL) character distribution, respectively, in the two annealed conditions. The 400°C annealed specimen show much higher CSL fraction (~0.54) as compared to the 600°C (~0.44) annealed specimen (Fig.4.5.6(a)). The CSL distribution (Fig.4.5.6(b)) in both the annealed conditions clearly indicates that most of the CSL boundaries have Σ3 character. The fraction of Σ3 boundaries is decidedly larger in the 400°C (~0.41) annealed specimen as compared to the 600°C (~0.35) annealed specimen.
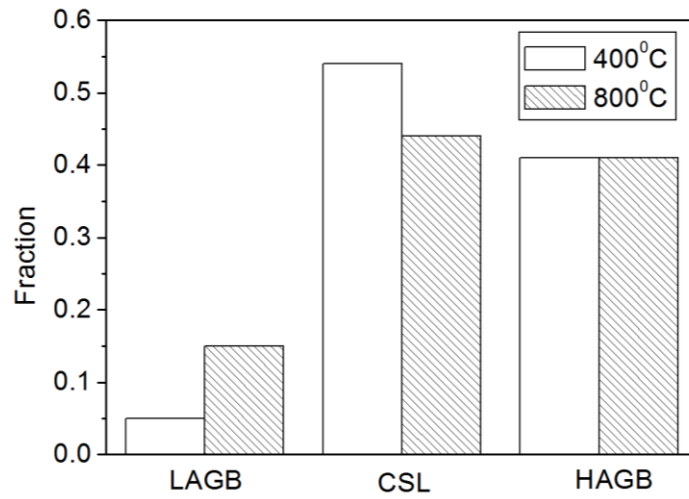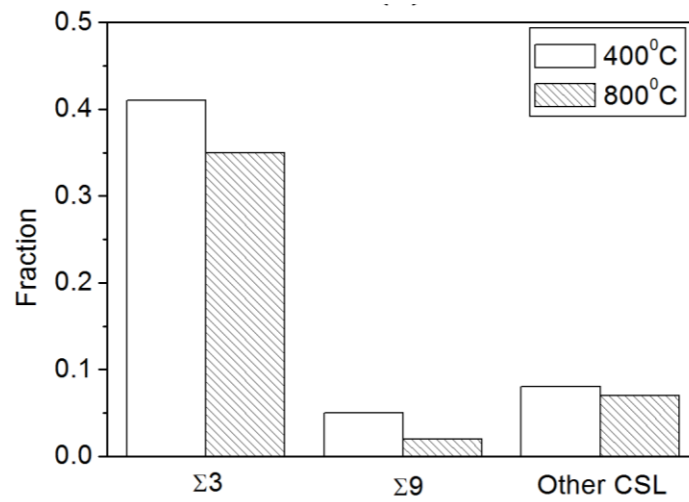
Figure 4.5.6: (a) GBCD and (b) CSL distribution of 90% deformed CCR processed nickel annealed at 400° and 800°C, respectively.

Chapter 5

Discussion

In the present work the effect of strain path change on the evolution of deformation and recrystallization texture has been critically investigated at different length scales using different characterization techniques. For the sake of clarity the deformation and recrystallization states will be analyzed separately in the following sections.

5.1 Evolution of Deformation Texture

The rolling texture SCR processed nickel is pure metal type which can be adequately described by the gradual evolution of a strong β fiber texture which is characterized by usually strong Cu, S and Bs components [4]. In contrast, in CCR processed nickel sample the deformation texture is characterized by the strong Bs and BsND orientations in heavily deformed condition. It might be noted that such strong Bs and rotated brass texture due to CCR processing has also been reported previously in copper and copper alloys [10].
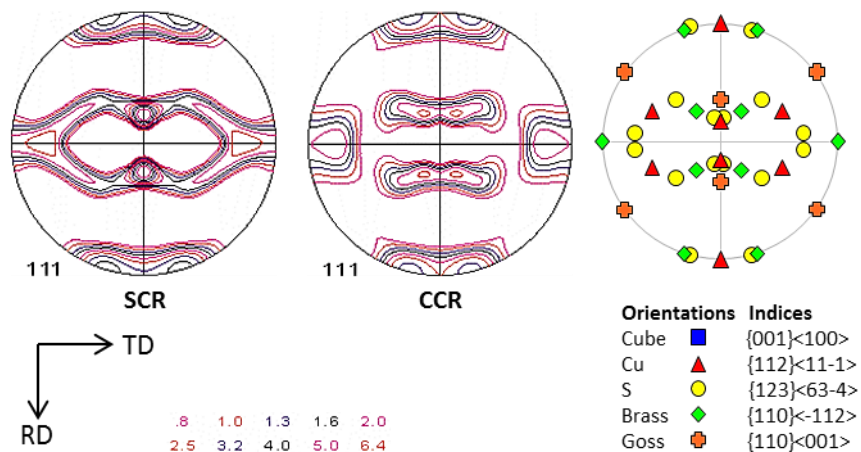

Figure 5.1.1: Experimental (111) PF of 90% deformed SCR and CCR processed and Nickel sample. The ideal locations of standard orientations considered have also been shown along with the PF.

Figure 5.1.1 shows the experimental (111) pole figure which indicated the difference in bulk texture of nickel for both procession route. The origin of deformation texture during deformation processing has been discussed from the view point of stability of different orientations in terms of the rotation field $\dot{R}\,(\dot{\varphi}_1, \dot{\varphi}_2, \dot{\varphi}_3)$ and the divergence of the rotation field $\left(\nabla.\dot{R} = \frac{d\dot{\varphi}_1}{d\varphi_1} + \frac{d\dot{\varphi}}{d\varphi} + \frac{d\dot{\varphi}_2}{d\varphi_2}\right)$ [24, 25]. The stability conditions are then given by $\dot{R} = 0$ and $\left(\nabla.\dot{R} \leq 0\right)$. The theoretical calculations of Hong et al [10] predict that amongst different texture components BsND would be stable under cross-rolling due to its higher inverse rotation rate and large negative divergence. The grains with orientations along the α-fiber will rotate to the Bs orientation (stable orientation during unidirectional rolling) and then will further rotate away to the BsND orientation when the direction of rolling is changed by 90° around the ND, thus, oscillating between the Bs and rotated brass orientation BsND which would be the two stable end orientations in CCR. This theoretical calculations agree well with their experimental results which show strong $\{011\} < 755 >$ orientation as the main component of deformation texture and spread around this orientations due to the oscillation between the two predicted stable end orientations. In the present case the strongest texture components as observed both from microtexture and bulk texture measurements are the Bs and Bs ND orientation $(01\,1)\,[21\,\overline{13}\,13]$ which is in fact very close to the orientation $\{011\} < 755 >$. The present experimental results thus agree quite well to the theoretical and experimental observations of Hong et al.

Previous investigations on CCR processed materials have shown the development of cube orientation as a minor texture component alongside the major component [8, 10, 20]. Although, development of cube texture is ruled out in the present case from the microtexture and bulk texture results, isolated cube oriented regions in form of thin band is clearly observed in the vicinity of locally sheared region in the EBSD map (Fig. 5.1.2) with characteristic spread around RD and TD denoted as C_{RD} and C_{TD} orientations in these band. Evidently, the volume fraction of cube component is rather small and as a result it is not immediately apparent in the PFs and ODFs.

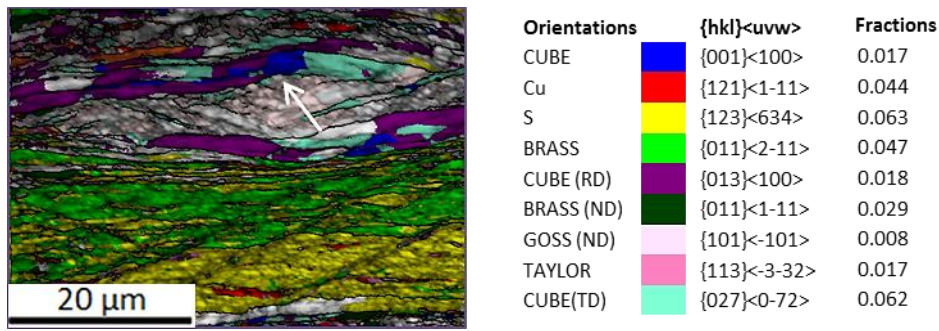| Orientations	{hkl}<uvw>	Fractions
CUBE	{001}<100>	0.017
Cu	{121}<1-11>	0.044
S	{123}<634>	0.063
BRASS	{011}<2-11>	0.047
CUBE (RD)	{013}<100>	0.018
BRASS (ND)	{011}<1-11>	0.029
GOSS (ND)	{101}<-101>	0.008
TAYLOR	{113}<-3-32>	0.017
CUBE(TD)	{027}<0-72>	0.062

Figure 5.1.2: IQ map with orientation showing the near cube orientations around shear region

It must be noted that while the CCR processing certainly affects the formation of deformation texture to a great extent, the present results indicate that the effect on microstructural refinement and consequently on the hardness properties are comparatively limited. This may be clearly understood from the gradual evaluation of key structural parameters such as HAGB spacing and average misorientation angle as shown in Fig. 5.1.3(a) and 5.1.3(b), respectively. It may be clearly seen the values are quite comparable for the SCR and CCR processed material in the heavily deformed condition (i.e. after 90% reduction in thickness). Consequently, the hardness properties (Fig.4.4.1) of the SCR and CCR processed materials are found to quite comparable in the heavily deformed condition. The slightly higher hardness in the 90% deformed SCR processed material is also consistent with the finer microstructure of this material as established by the values of different structural parameters.
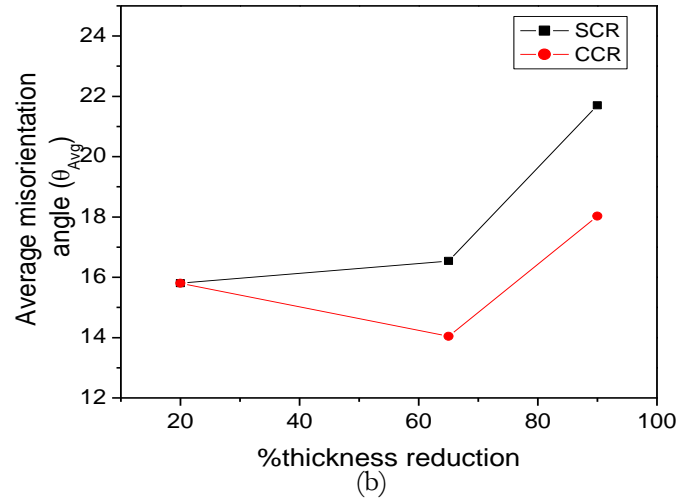

(a)
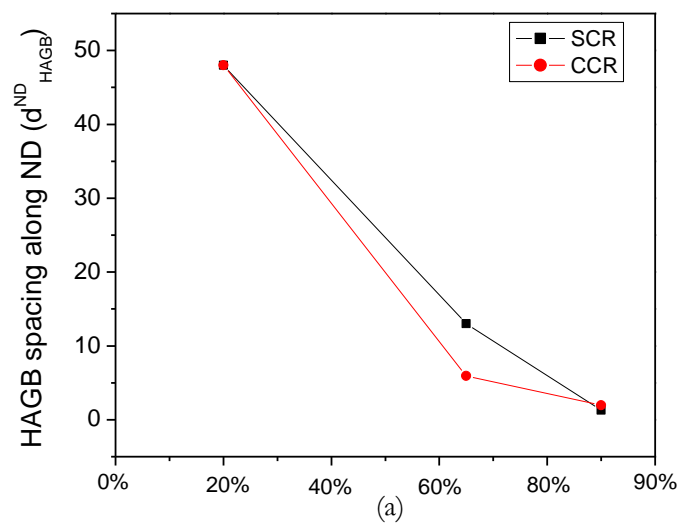
Fig. 5.1.3: Variation of (a) HAGB spacing along ND (d^{ND}_{HAGB}) and (b) average misorientation angle (θ_{Avg}) with imposed strain

5.2   Evolution of Recrystallization Texture

The recrystallization texture of heavy cold rolled, SCR processed Ni is widely reported as a strong Cube texture, the explanation of such a sharp texture is given by based on two contending theories namely, oriented nucleation and oriented growth based on a relative importance of nucleation and growth stages in development of recrystallization textures. In contrast the recrystallization texture of heavily rolled CCR processed Ni is composed of ND || <111> fiber texture after low temperature annealing (at 400°C for 1 hr.) which weakens at high temperature annealing (at 800°C for 1 hr.).

From the microtexture map shown in Fig. 5.2.1 (a) it can be observed that the spatial distribution of $(445)\,[13\overline{2}38]$ (light blue colour) orientation is always adjacent to the TD oriented cube grains $(027)[0\overline{7}2]$ (aqua colour) which is separated $\Sigma3$ annealing twin boundaries (red lines). This indicates that the origin of this orientation is the twinning of the parent TD oriented cube grains (C_{TD}), hence it is denoted as C_{TD}^{T} .
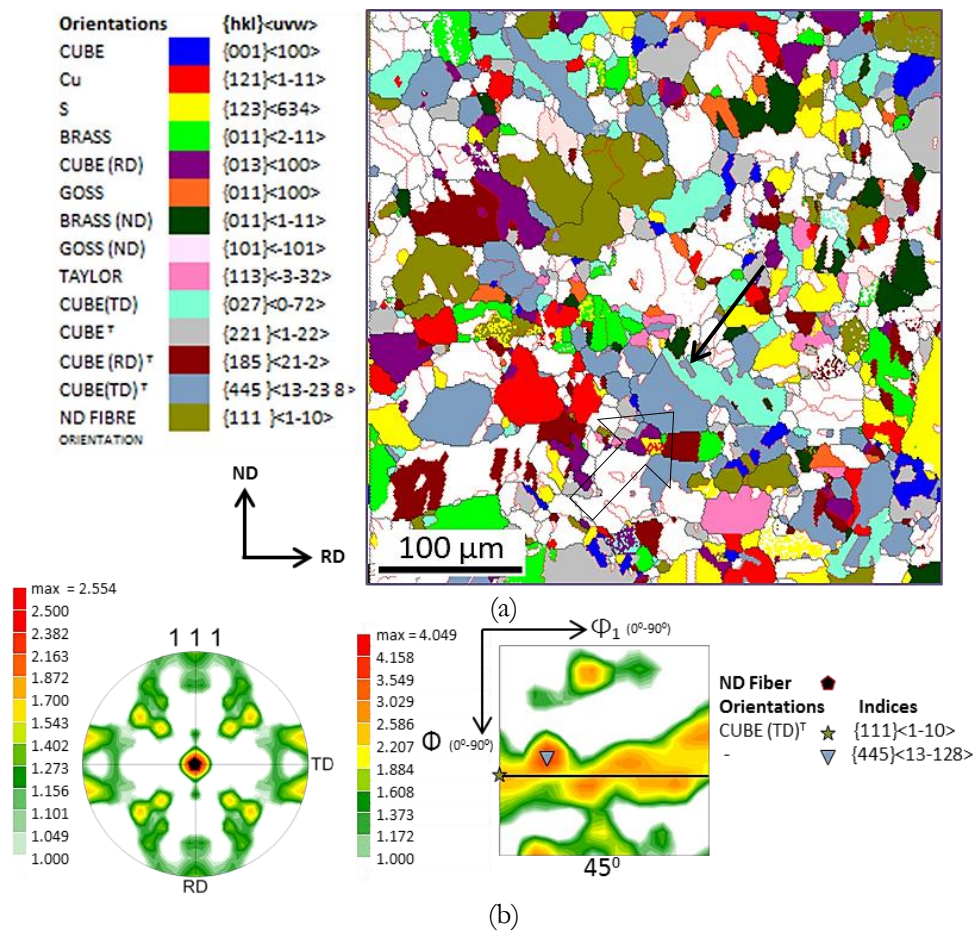
Figure 5.2.1: (a) GO maps (b) Experimental (111) PF and ODF section φ_2= 45° of Nickel sample which is CCR processed 90% deformed and subsequently annealed at 400°C for 1 hr.

In ODF section $\varphi_2 = 45°$ (Fig. 5.2.1(b)) is can be seen that C_{TD}^T is prominent orientation of ND || <111> fiber tube along with $(111)[1\bar{1}0]$. The propensity for annealing twin formation during recrystallization may be related to the growth stagnation. The growth stagnation may occur when the growing recrystallized grains are isolated from the deformed matrix by low misorientation boundaries which have been demonstrated by in-situ experiments [21]. Occurrence of twinning becomes favourable due to the fact that twinning can reorient the parent grains to alter the local misorientation so that growth can continue. The situation might be understood from the orientation map in Fig.5.2.1. The C_{TD}^T grain shown by block arrow has the same orientation as the two small twin grains in the adjacent parent C_{TD} grain. Following the in-situ EBSD observations of Field et al [21] it appears that the C_{TD}^T grain might have nucleated from the boundary of the parent C_{TD} grain due to growth stagnation and with progressing recrystallization has become independent of the parent C_{TD} and thus finally appears as an independent grain in the microstructure. To further elucidate this fact the orientations map obtained after short time annealing treatment (10 seconds at 350°C) is presented in Fig.5.2.2. The recrystallized grains are observed clearly in still deformed matrix (masked black). The distribution of orientation is rather diverse but presence of the C_{TD} grains are noticed along with recrystallized grains of other orientations. The early recrystallized C_{TD} grains are already found to be separated from its twin orientation C_{TD}^T by $\Sigma 3$ boundaries an example of which is shown by the yellow arrow mark. It is thus quite reasonable that this twinned grains grow independent of parent finally giving rise to the observed ND||[111] fiber microtexture. It may be noted that the microtexture results of 400°C annealed CCR processed Ni bear resemblance to the recrystallization texture of cross rolled copper which consists of a weak cube component and twin of the cube component as has been reported by Ozturk [8]. Of course, in the present case rather than cube oriented grains mostly C_{TD} and twin of this orientation i.e. C_{TD}^T or $\{445\} < 13\,\overline{23}8 >$ are observed.
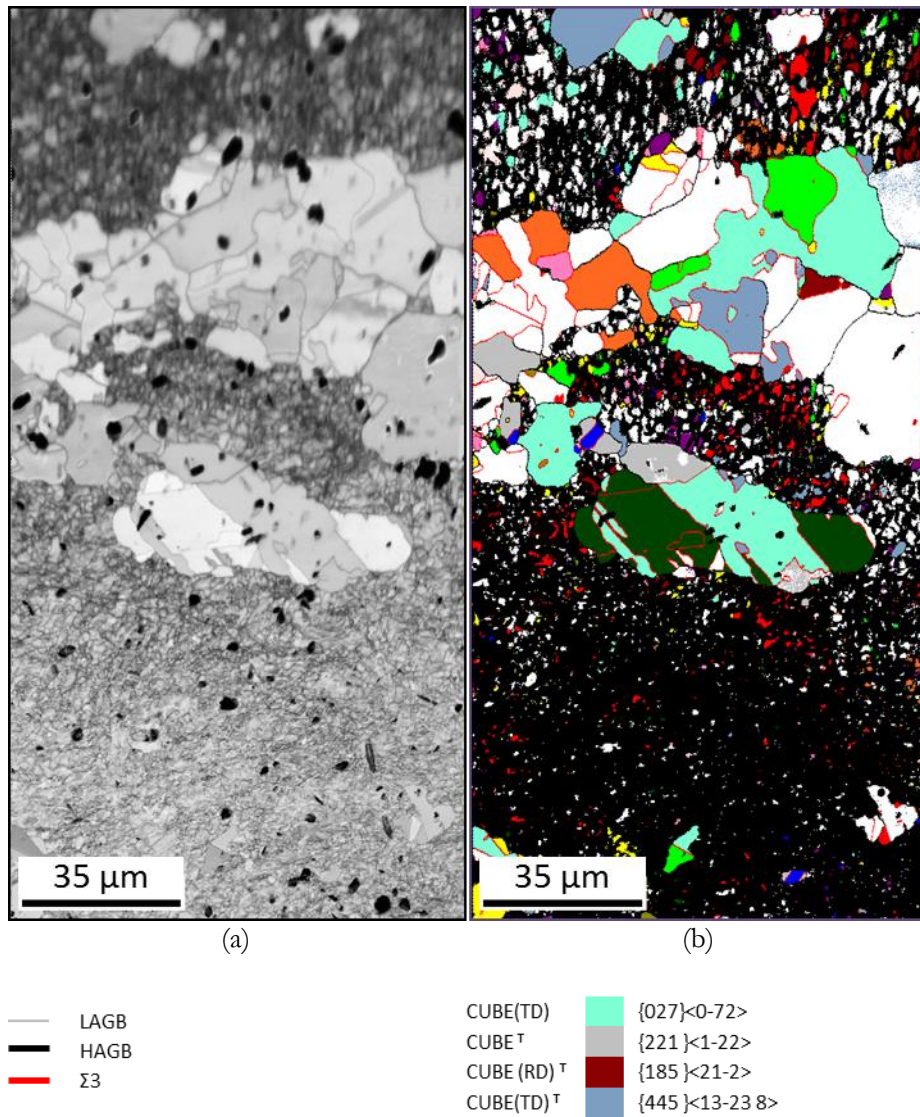
Figure 5.2.2: (a) IQ map (b) GO map of Nickel sample which is CCR processed 90% deformed and subsequently annealed at 350°C for 10 seconds.

The weakening of this microtexture in high temperature annealing appears to be also in agreement with decreased propensity for twin formation as also clearly evidenced in the comparative GBCD plot (Fig. 4.5.6 (a)) of 400° and 800°C annealed conditions which shows drop in the CSL fraction in the 800°C annealed condition due to the drop in the $\Sigma 3$ annealing twin boundary fraction (Fig.4.5.6 (b)).

The present results are in good agreement with those of Field et al [21] who observed higher twin densities develop at lower annealing temperatures on the formation of annealing twins during recrystallization of Cu. It is proposed that at higher annealing temperatures the growth

of the grains should be less dependent on twinning as the thermal energy should be adequate to meet the required driving force. Thus, the newly recrystallized grains can grow free of hindrance. Support for this observation is obtained from the presence of large twin-free C_{TD} oriented grains in the orientation map of 800°C annealed specimen.

The failure to observe the formation of strong cube texture in recrystallized cross-rolled Ni remains interesting from the mechanistic point of view. Merlini et al [20] have explained the absence of cube texture in cross-rolled copper through the oriented growth model and discarded the role of oriented nucleation due to the fact that cube regions exist in the deformed structure but strong cube texture formation is not observed up on annealing. Strong preferential nucleation of near cube oriented grains is not observed in the present study as well. However, absence of preferential nucleation of cube grains leading to the absence of a strong final cube texture may be interpreted as a support to the oriented nucleation theory but in a negative sense. It is to be kept in view that internal structure of the cube bands and local misorientation environment are far more important factors than mere presence of large cube oriented regions in deformed microstructures as shown recently by Bhattacharjee et al [22]. The preferential nucleation of cube grains is aided by the already recovered structure of the cube grains due to the special arrangement of gliding dislocations with orthogonal burgers vector [23]. The substructure destabilization during cross-rolling can affect the attainment of a recovered structure in near cube oriented regions so crucial for early nucleation. Indirect evidence for this could be obtained in the IQ distribution map (Fig. 5.2.3(c)) of the region surrounding the cube band of Fig.5.2.3 (a), cropped and reproduced in Fig.5.2.3 (b), which gives an indirect estimate of the distribution of stored energy. It may be clearly observed that the C_{TD} oriented regions has much higher IQ than adjacent near C oriented regions indicating more recovered structure of the former. Incidentally, more C_{TD} oriented grains are actually observed in the annealed materials as already discussed. Further, the cube oriented regions are also observed at the vicinity of the locally sheared regions which can also plays an important role due to their adverse impact on the nucleation and growth of cube grains [15,23]. Further investigations are planned to study in detail the internal structure of the cube regions and local misorientation environment in cross-rolled nickel to clarify these issues.

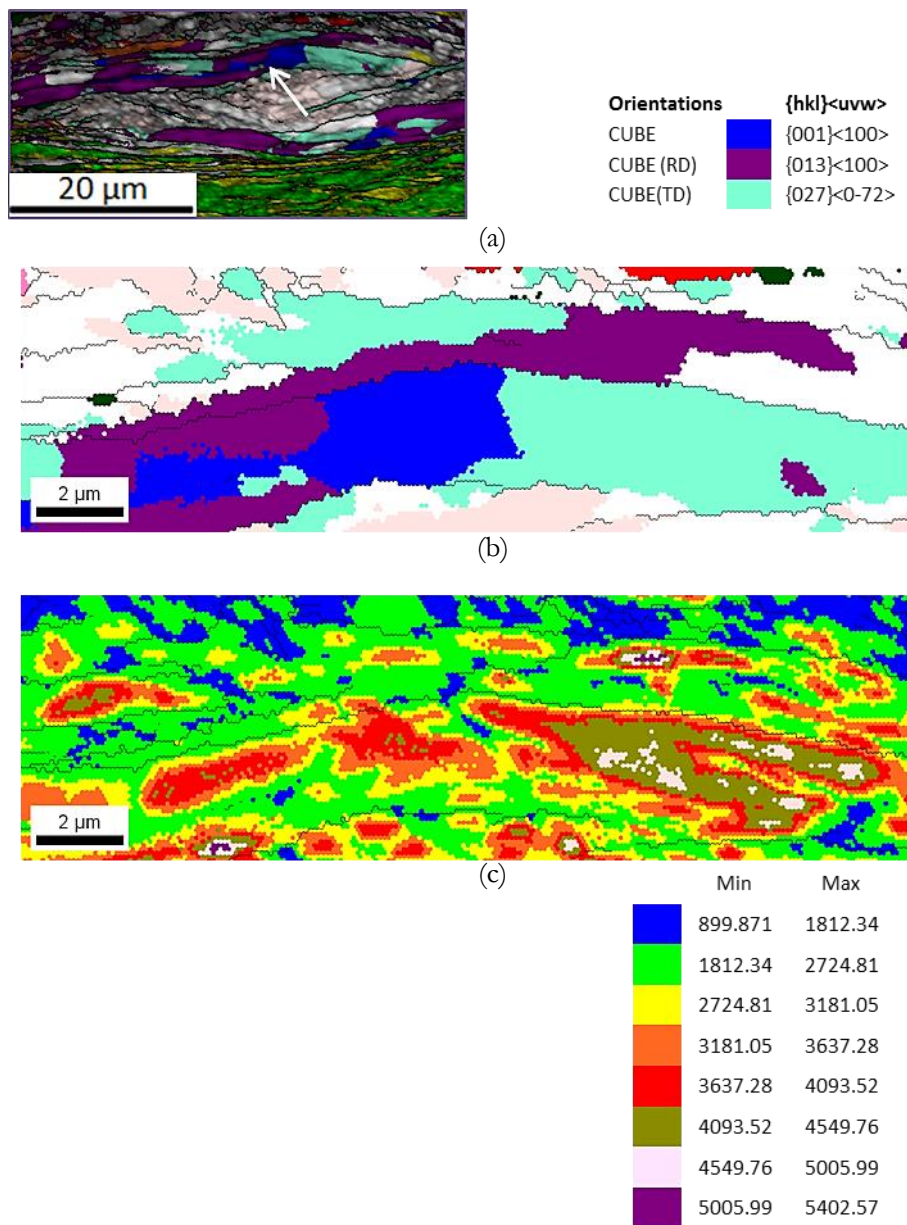|	Min	Max
	899.871	1812.34
	1812.34	2724.81
	2724.81	3181.05
	3181.05	3637.28
	3637.28	4093.52
	4093.52	4549.76
	4549.76	5005.99
	5005.99	5402.57

Figure 5.2.3: (a) IQ map showing of shear region surrounded by cube oriented bands (b) GO map of cube oriented region (c) IQ distribution map of corresponding regions of 90% CCR processed Nickel sample.

Chapter 6

Summary and Conclusions

In order to understand the effect of strain path change on the evolution of deformation and recrystallization texture, high purity nickel with 36 μm starting grain size has been deformed by two separate processing routes namely SCR and CCR up to 90% reduction in thickness followed by annealing at different temperatures ranging between 400° to 800°C. The microstructure and texture of the processed materials have been characterized at different length scales using X Ray Diffraction and EBSD. The following conclusions may be drawn from the present study:

1. The microstructure of CCR processed samples were intersecting shear bands and shear regions enclosed within banded structures.

2. The texture of CCR processed nickel is characterized by the strong presence of Bs and Bs^{ND} components and agrees well with the theoretical predictions and experimental observations in other medium to high stacking fault energy fcc materials.

3. The microtexture after low temperature annealing (at 400°C for 1hr.) shows a ND||[111] fiber. It is strongest at orientation $(445)[13\overline{2}38]$ which is thought to originate from the twinning of the TD-rotated cube component $(027)[0\overline{7}2]$. This is also confirmed from early stages of recrystallization.

4. The twin formation is favoured during low temperature annealing supposedly due to the fact the reorientation during twin can assist in eliminate the growth stagnation.
   After high temperature annealing the ND||[111] fiber is weakened. This agrees well with decreased twinning activity at higher annealing temperatures. The texture is also the annealing texture is weak and rather diffuse.

5. Preferential nucleation of near cube grains is not observed at early stages of recrystallization in cross-rolled nickel leading to the formation of a weak and diffuse cube texture up on completion of recrystallization.

6. The internal structure and local misorientation environment of cube regions in cross-rolled nickel appear to be important factors for this behavior but needs to be investigated further in detail.

References

[1] S. Suwas and A. K. Singh. Role of strain path change in texture development. Materials Science and Engineering A 356.1-2, (2003) 368-371.

[2] R. E. Bauer. Rudolf, Heinrich Mecking, and Kurt Lücke. Textures of copper single crystals after rolling at room temperature. Materials Science and Engineering 27.2, (1977) 163-180.

[3] J. Hirsch, K. Lücke, and M. Hatherly. Overview No. 76. Mechanism of deformation and development of rolling textures in polycrystalline f.c.c. Metals-III. The influence of slip inhomogeneities and twinning. Acta Metallurgica 36.11, (1988) 2905-2927.

[4] J. Hirsch and K. Lücke. Overview no. 76. Mechanism of deformation and development of rolling textures in polycrystalline f.c.c. metals-I. Description of rolling texture development in homogeneous CuZn alloys. Acta Metallurgica 36.11, (1988) 2863-2882.

[5] R. K. Ray. Rolling textures of pure nickel, nickel-iron and nickel-cobalt alloys. Acta Metallurgica Et Materialia 43.10, (1995) 3861-3872.

[6] T. Leffers and R. K. Ray. The brass-type texture and its deviation from the copper-type texture. Progress in Materials Science 54.3, (2009) 351-396.

[7] N. P. Gurao, S. Sethuraman and Satyam Suwas. Effect of strain path change on the evolution of texture and microstructure during rolling of copper and nickel. Materials Science and Engineering A 528.25–26, (2011) 7739-7750.

[8] T. Ozturk. Deformation and recrystallization textures in cross rolled sheets of copper and alpha Brass. Scripta Metallurgica 22.4, (1988) 1611-1616.

[9] T. O. Suet, W. B. Lee and B. Ralph. Deformation and recrystallization in cross- rolled AI-Cu precipitation alloys. Journal of Materials Science 29, (1994) 269-275.

[10] Seung-Hyun Hong and Dong Nyung Lee. Deformation and Recrystallization Textures in Cross-Rolled Copper Sheet. Journal of Engineering Materials and Technology 124.1, (2002) 13-22.

[11] O. Engler. Recrystallisation textures in copper-manganese alloys. Acta Materialia 49.7, (2001) 1237-1247.

[12] P. P Bhattacharjee, R. K. Ray, and A. Upadhyaya. Development of cube texture in pure Ni, Ni-W and Ni-Mo alloys prepared by the powder metallurgy route. Scripta Materialia 53.12, (2005) 1477-1481.

[13] P. P. Bhattacharjee and R. K. Ray. Effect of processing variables on cube texture formation in powder metallurgically prepared Ni and Ni-W alloy tapes for use as substrates for coated conductor applications." Materials Science and Engineering A 459.1-2, (2007) 309-323.

[14] K. Kashyap and R. George. Mechanism of cube grain nucleation during recrystallization of deformed commercial purity aluminum. Bulletin of Materials Science 29.2, (2007) 197-200.

[15] P. P. Bhattacharjee, R K Ray and N Tsuji. Cold rolling and recrystallization textures of a Ni–5at.% W alloy. Acta Materialia 57.7, (2009) 2166-2179.

[16] R. Penelle. Nucleation and growth during primary recrystallization of certain metals and alloys with a face-centered cubic structure: Formation of the cube texture. International Journal of Materials Research 100.10, (2009) 1420-1432.

[17] Pinaki P. Bhattacharjee, Ranjit K. Ray, and Nobuhiro Tsuji. Evolution of Deformation and Recrystallization Textures in High-Purity Ni and the Ni-5 at. pct W Alloy. Metallurgical and Materials Transactions A 41.11, (2010) 2856-2870.

[18] A. L. Helbert. W. Wang, T. Baudin, F. Brisset and R. Penelle. Formation and development of strong cube recrystallization texture in an aluminium of commercial purity. Materials Science Forum, (2012) 391-397.

[19] M. Y. Huh, S. Y. Cho and O. Engler. Randomization of the annealing texture in aluminum 5182 sheet by cross-rolling. Materials Science and Engineering A 315.1–2, (2001) 35-46.

[20] A. Merlini and P. A. Beck. Study of the origin of the cube texture. Acta Metallurgica 1.5, (1953) 598-606.

[21] D.P. Field, L.T. Bradford, M.M. Nowell and T.M. Lillo. The role of annealing twins during recrystallization of Cu. Acta Materialia 55, (2007) 4233–4241.

[22] P. P. Bhattacharjee, Y. Takatsuji, Y. Miyajima, D. Terada, , N Tsuji. Evolution of Microstructure and Texture During Cold Rolling and Annealing of a Highly Cube-Textured ({001} Formula Not Shown) Polycrystalline Nickel Sheet. Metallurgical and Materials Transactions A 43, (2012) 2442 – 2452.

[23] A.A. Ridha and W.B. Hutchinson. Recrystallisation mechanisms and the origin of cube texture in copper. Acta Metallurgica 30, (1982) 1929-1939.

[24] J. Savoie and J.J. Jonas. Simulation of the deformation textures induced by Deep-Drawing in extra low-carbon steel sheets. Acta metallurgica et materialia 42.12, (1994) 4101-4116

[25] L S Tóth, J J Jonas,D Daniel,R K Ray. Development of ferrite rolling textures in low and extra low carbon steels. Metallurgical Transactions 21A, (1990) 2985–3000.

[26] A. D. Rollett and P. N. Kalu. Typical Textures in FCC Metals. Lecture slides: Texture, Microstructure & Anisotropy. Carnegie Mellon University, USA 2007.